Available online at www.sciencedirect.com

ScienceDirect

Journal of Nutritional Biochemistry 120 (2023) 109409

Journal of Nutritional Biochemistry

RESEARCH PAPER

# Butyrate restores the fat/lean mass ratio balance and energy metabolism and reinforces the tight junction-mediated intestinal epithelial barrier in prediabetic mice independently of its anti-inflammatory and epigenetic actions

Valquiria A. Matheus[a,*], Ricardo B. Oliveira[a], Daniela A. Maschio[a,b], Susely F.S. Tada[a], Gabriela M. Soares[b], Felippe Mousovich-Neto[a], Raul G. Costa[a], Marcelo A. Mori[a,b], Helena C.L. Barbosa[b], Carla B. Collares-Buzato[a,*]

[a] Department of Biochemistry and Tissue Biology, Institute of Biology, University of Campinas (UNICAMP), Campinas, São Paulo, Brazil
[b] Obesity and Comorbidities Research Center, Institute of Biology, UNICAMP, Campinas, Brazil

Received 7 March 2023; received in revised form 24 May 2023; accepted 21 June 2023

**Abstract**

Tissue/cellular actions of butyrate on energy metabolism and intestinal barrier in normal metabolic conditions or prediabetes are still unclear. In this work, we investigated the beneficial effect of dietary supplementation with sodium butyrate on energy metabolism, body mass composition, and intestinal epithelial barrier mediated by tight junction (TJ) in chow diet-fed normal and high-fat diet (HF)-fed prediabetic mice, considering the well-known butyrate action as an epigenetic and inflammatory regulator. Butyrate significantly reduced the fat/lean mass ratio, slightly ameliorated dyslipidemia, restored oral glucose tolerance, and increased basal energy expenditure in prediabetic HF-fed mice but had no effect on control animals. Such effects were observed in the absence of significant alterations in the hypothalamic expression of orexigenic and anorexigenic genes and motor activity. Also, butyrate suppressed the whitening effect of HF on brown adipose tissue but did not affect cell bioenergetics in immortalized UCP1-positive adipocytes *in vitro*. Butyrate reinforced the intestinal epithelial barrier in HF-fed mice and in Caco-2 monolayers, which involved higher trafficking of TJ proteins to the cell-cell contact region of the intestinal epithelia, without affecting TJ gene expression or the acetylation level of histones H3 and H4 *in vivo*. All metabolic and intestinal effects of butyrate in prediabetic mice occurred in the absence of detectable changes in systemic or local inflammation, or alterations in endotoxemia markers. Butyrate has no effect on chow diet-fed mice but, in the context of HF-induced prediabetes, it prevents metabolic and intestinal dysfunctions independently of its anti-inflammatory and epigenetic actions.


*Keywords:* Butyrate; Type 2 prediabetes; High-fat diet; Intestinal epithelial barrier; Inflammation.

## 1. Introduction

Type 2 diabetes mellitus (T2D) is the most frequent form of diabetes, accounting for approximately 90% of the diagnosed cases, and is recognized as a serious global health issue [1]. T2D is primarily the result of the insensitivity of target tissues to the action of insulin (known as peripheral insulin resistance), which leads to hyperglycemia [2,3]. Obesity and its associated conditions, such as dyslipidemia, are positively associated with high systemic concentrations of inflammatory biomarkers (*i.e.*, TNF-alpha, IL-1, IL-6, IL-10), which, in conjunction, are predictive of insulin resistance and the incidence of T2D [4,5]. The combination of hyperglycemia and high free fatty acids (FFAs) is directly related to the onset and aggravation of the insulin resistance state as well as beta-cell dysfunction during T2D [3,6]. White adipose tissue (WAT) plays an important role in T2D pathogenesis since it controls the levels of circulating FFAs and releases cytokines and inflammatory factors that impair insulin signaling [4]. Meanwhile, brown adipose tissue (BAT) consumes high levels of glucose and lipids when activated, and thus can counteract hyperglycemia and hyperlipidemia in T2D [7].

*Abbreviations:* T2D, Type 2 Diabetes Mellitus; BAT, Brown Adipose Tissue; WAT, White Adipose Tissue; SCFA, Short-Chain Fatty Acid; TJ, Tight Junction.

This work was funded by grants from FAPESP (Grant numbers 2018/02118-2 and 2017/01184-9, Brazil), CAPES (Financial code 001, for the scholarship awarded to VAM), and CNPq (Grant number 308546/2018-0, Brazil).

* Corresponding authors at: R. Monteiro Lobato, 255, 13083-970 Campinas, São Paulo, Brazil. Tel.: +55 19 35216246.
*E-mail addresses:* valviski@gmail.com (V.A. Matheus), collares@unicamp.br (C.B. Collares-Buzato).

https://doi.org/10.1016/j.jnutbio.2023.109409
0955-2863/

Several studies have also suggested an involvement of intestinal microbiota and dysfunction of the intestinal epithelial barrier in the pathogenesis of obesity-associated T2D [8–13]. According to this hypothesis, changes in the intestinal microbiota can lead to an increase in the proportion of Gram-negative bacteria associated with intestinal barrier impairment, favoring the absorption of lipopolysaccharides (LPS) and other toxins, and, consequently, the induction of metabolic endotoxemia that aggravates peripheral insulin resistance [14,15].

One of the main components of what constitutes the intestinal barrier is the selectively permeable intestinal epithelium, composed of a monolayer of juxtaposed columnar epithelial cells that separates the luminal environment from the internal environment [16]. There are two ways in which ions and molecules (including nutrients) can pass through the intestinal epithelial monolayer, *i.e.*, the transcellular and the paracellular routes [16]. The integrity of the paracellular pathway depends on the regulation of the protein complex associated with the tight junction (TJ), where an apparent fusion of the plasma membranes of adjacent cells occurs [16]. The TJ complex is composed of integral proteins, such as occludin and those belonging to the claudin family, which interact indirectly with the perijunctional ring of actin cytoskeleton through cytoplasmic proteins such as zonula occludens - ZO-1, ZO-2, and ZO-3, cingulin, and 7H6 antigen, among others [16–19].

There has been an increasing interest in alternative therapies for T2D using nutrients and natural substances that act against the processes that trigger/aggravate insulin resistance, such as the excess of circulating glucose and FFAs, the release of cytokines and inflammatory factors by the WAT, and the entrance of substances from an altered microbiota into the circulation through a disrupted intestinal barrier [9,20,21]. Sodium butyrate is a short-chain fatty acid (SCFA) produced by the intestinal microbiota (mainly in the colon) as the consequence of fermentation of nondigestible carbohydrates [22–24]. Several studies have shown that butyrate supplementation has metabolic benefits and anti-inflammatory actions in animal models of T2D [22,25–30], while the production of this SCFA is reduced in diabetic patients [22].

Previous results from our group showed that supplementation with sodium butyrate ameliorates insulin resistance and improves parameters associated with glucose intolerance, hepatic steatosis, and intestinal barrier dysfunction in prediabetic C57BL6 mice fed a high-fat diet [31]. This SCFA has also shown a beneficial effect on gastrointestinal function [32] and, under *in vitro* conditions, reinforced the epithelial barrier by increasing the gene expression of TJ proteins [33]. We have also observed that diet supplementation with butyrate significantly inhibited the decrease in claudin-1 junctional content in intestinal epithelia of prediabetic mice [31].

It has been suggested that part of the cellular effects of butyrate results from its action as an epigenetic regulator through inhibition of the histone deacetylase (HDAC) [23,34–36]. It was demonstrated, for instance, that the regulation of cell growth mediated by this SCFA occurs via the activation or inactivation of genes related to cell proliferation [37]. In addition, butyrate and other SCFAs are well known for their anti-inflammatory actions, which can explain, at least in part, their effects on metabolism [38–40].

However, studies to investigate the effect of butyrate on energy metabolism and intestinal barrier at normal metabolic conditions or the early stages of T2D (prediabetes) are scarce [25,31]. Also, the mechanisms underlying the protective action of butyrate on the TJ-mediated intestinal barrier disruption in prediabetic mice remain unknown. Therefore, the objective of this work was to further investigate the beneficial effect of sodium butyrate on energy metabolism, fat/lean body mass, and the intestinal epithelial barrier mediated by tight junction (TJ) in chow diet-fed mice and in *in vitro* and *in vivo* model of type 2 prediabetes, considering its action as an epigenetic and inflammatory regulator.

To extend our previous findings [31], we evaluated herein the effect of butyrate on dyslipidemia, body composition (by microtomography), basal energy expenditure (EE), as well as gene expression of *Ucp1* in BAT and orexigenic/anorexigenic genes in the hypothalamus of C57BL6/Unib mice fed a chow or high-fat (HF) diets. As an *in vitro* model of the epithelial intestinal barrier, we employed the human colorectal adenocarcinoma cell line Caco-2, which displays many physiological and morphological features of mature enterocytes [41,42]. The function and structure of the intestinal epithelial barrier, in both *in vivo* and *in vitro* models, were assessed by measuring the paracellular flux with the marker Lucifer Yellow (LY), and by analyzing the cellular distribution and expression of proteins associated with TJ (namely, claudin-2 and -3, occludin, and ZO-1) by immunofluorescence, immunoblotting, and qPCR. The degree of acetylation of histones H3 and H4 in cryosections of the intestinal epithelium was also measured, as well as the plasma/serum and intestinal concentrations of LPS, TNF-$\alpha$, IL-6, and zonulin (a known endogenous modulator of the TJ-associated intestinal barrier) [43–45]. Finally, given the possible therapeutic use of butyrate as an adjuvant in the treatment of metabolic and intestinal diseases, we have also investigated the effect of butyrate on hematological and biochemical parameters in the animals of the different experimental groups.

## 2. Materials and Methods

### *2.1. Animals, treatments, and metabolic/biochemical/hemogram analyzes*

Male C57BL/6JUnib mice, aged 16–18 weeks, were obtained from the breeding colonies of the Multidisciplinary Center for Biological Investigation on Laboratory Animal Science (CEMIB) at the University of Campinas (UNICAMP, Brazil). They were maintained in micro isolator cages under controlled conditions of temperature (22 ± 1°C)/humidity, and a 12 h-light/12 h-dark cycle and had free access to food and water during the entire experimental period (60 days). Sodium butyrate (cat# 303410, Sigma-Aldrich) was incorporated into a regular diet or a hypercaloric high-fat content (HF) diet at the concentration of 5% (w/w) [31]. Mice were divided into four experimental groups: (1) Control group (C), received a standard rodent diet (Nuvilab, Quintia - in powder; containing 4.5% lipids, 53% carbohydrates, and 23% proteins, w/w; 11.8% of calories in lipids); (2) Control + Butyrate group (CB), received the standard diet mixed with 5% of sodium butyrate (w/w); (3) High-fat group (HF), received a prepared high-fat diet (in powder; containing 21% lipids (mainly lard and soy oil), 50% carbohydrates, and 20% proteins, w/w; 40.3% of calories in lipids); (4) High-fat + Butyrate group (HFB), received the prepared high-fat diet mixed with 5% of sodium butyrate (w/w).

The following parameters were evaluated in the animals: the body weight gain, the weight of the retroperitoneal (rWAT) and epididymal white adipose tissue (eWAT) and the interscapular brown adipose tissue (iBAT), the fast and fed glycemia and the lipidemia (plasma concentration of triglycerides, cholesterol, HDL, and LDL) and response to the glucose tolerance test (oral GTT, expressed as area values under the curve). These procedures were performed as previously described [46–48]. The blood glucose concentration was measured using an Accu-Chek Active glucometer (Roche Diagnostic, Switzerland). Lipidemia was measured using commercial kits (Enzymatic Colestat AA liquid, LDL Cholesterol Reactive Precipitant, HDL Cholesterol Reactive Precipitant, and TG Color GPO/PAP AA, Weiner Lab., St. Ingbert-Germany).

Blood samples were also obtained for hematology/hematocrit analysis and biochemical parameters (such as amylase, alanine aminotransferase (ALT), aspartate aminotransferase (AST), and creatinine) performed by a specialized veterinary laboratory (VetPat, Campinas, SP, Brazil).

All the experiments were approved by the Institutional Committee for Ethics in Animal Experimentation of the University of Campinas (CEUA/UNICAMP; under Protocol: 4185-1).

### 2.2. Evaluation of fat/lean mass ratio, the basal energy expenditure, and locomotor activity

The measurement of the basal EE was performed using a metabolic chamber system (Oxylet—Panlab/Havard Apparatus, Barcelona, Spain). After 3 h of adaptation, the mice were monitored, and the data was recorded for a period of 48 h. The basal locomotor activity was measured for 24 h using a cage system coupled to the equipment that counts each movement (Physiocage - Panlab/Havard Apparatus, Spain). For both procedures, mice from the different experimental groups were housed individually under a light and dark cycle of 12 h at 24°C, with free access to water and food [49]. The computerized microtomography technique (Micro-CT) was used to evaluate the fat and lean masses per total body mass [50,51]. Anesthetized mice (with 80 mg/kg ketamine hydrochloride and 10 mg/kg xylazine hydrochloride, intraperitoneal injection) were placed in the micro-CT scanner (Bruker - Skyscan 1178 - USA). The X-Ray energy parameters were: 44 kV; 150 $\mu$A; 6.6 W. One thousand images were obtained along at 360° rotation, followed by the reconstruction of these images to create a 3D image using the program NRecon version 1.6.10.2 (SkyScan, USA) and the Feldkamp algorithm. The region of interest was determined according to differences in tissue radiodensity and processed accordingly to measure relative volumes of fat and lean masses. The values of relative fat mass and lean mass were expressed as a percentage of the total volume of adipose tissue and total skeletal muscle, respectively, in relation to the total body volume.

### 2.3. Histological analysis of intestinal segments and BAT

Fragments of the intestine (jejunum, ileum, and colon) and BAT obtained from each experimental group were fixed in a 4% paraformaldehyde solution, and then paraffin-embedded, sectioned (5 μm thickness), and processed for Hematoxylin-Eosin (HE) staining. Images were obtained using an optical microscope (Nikon Eclipse E-400 - Nikon, Japan) coupled to a digital camera (Olympus U-TV 0.5 C-3, Olympus Corporation, Waltham, USA). For the morphometry of the BAT, a total of 10 images were randomly captured from two different sections per animal using the same magnification (40× objective lens) and image capture parameters of the microscope. The area for lipid droplets was quantified and expressed relative to the total image area by using ImageJ (http://rsbweb.nih.gov/ij/).

### 2.4. Quantitative real-time PCR in hypothalamus and BAT fragments

Total RNAs were extracted from the total hypothalamus and fragments of BAT using TRIzol. The reverse transcription in cDNA was performed using the Superscript II kit (Invitrogen, Carlsbad, CA, USA). Quantitation of mRNAs was performed using the Real-Time PCR System 7500 with the Master Mix SYBR Green PCR (AppliedBiosystems, Carlsbad, CA, USA). Primer sequences used are shown in Table S1 (Supplementary Material). Absolute amounts of mRNAs of interest were normalized by the control gene Hypoxanthine-guanine phosphoribosyltransferase (HPRT), using the $2^{-\Delta\Delta Ct}$ method [52].

### 2.5. Cultured 9W adipose cell line, treatment, cell viability, and bioenergetics

Immortalized adipocyte precursor cells isolated from subcutaneous inguinal adipose tissue - 9W cells - were used in this study to evaluate butyrate effects on cellular bioenergetics. Cells were cultured in 90 × 15 mm plates on DMEM high glucose supplemented with 10% fetal bovine serum (Gibco) and 1% streptomycin and penicillin (Gibco) and kept in an incubator at 37°C with 5% $CO_2$ and 70% humidity. After confluency (8 days), cells were used for experiments (for undifferentiated cells) or induced to differentiate into 9W beige adipocytes by the addition of adipogenic medium as previously described [53]. Undifferentiated or differentiated 9W cells were treated for 6 or 24 hours with 0.5 mM of sodium butyrate diluted in high-glucose DMEM. This concentration of butyrate was chosen based on the following premises: (1) it is within the physiological concentration range [54], and (2) it has no apparent cytotoxicity besides displaying biological effects on different cell types in vitro [55,56]. The cell viability after butyrate treatment was assessed using the MTT assay and absorbance was measured at 570 nm using a microplate reader (PowerWave XS2) [53]. Cellular bioenergetics of the 9W cells (undifferentiated and differentiated) were measured by high-resolution respirometry (Oroboros Oxygraph-O2K, Oroboros Instruments, Innsbruck, Austria) at 37°C in Krebs-Ringer pH 7.4 (NaCl 130 mM, KCl 4.7 mM, 1.24 mM $MgSO_4$, 2.5 mM $CaCl_2$, 10 mM HEPES, 2.5 mM $NaH_2PO_4$, 2% BSA). Cells at a density of $8 \times 10^5$ (differentiated) or $1.5 \times 10^6$ (undifferentiated) were added to oxygraph chambers to obtain oxygen consumption fluxes according to a previously published protocol [57]. Briefly, oligomycin (2 μg/mL) was added into the chambers aiming to obtain ATP-dependent and proton leak oxygen consumption. Afterward, mitochondrial uncouplers were tritiated (0.05 μM per addition) – CCCP (Carbonylcianeto m-chlorophenylhydrazone) or FCCP (Carbonyl cyanide-4-(trifluoromethoxy) phenylhydrazone – to reach maximal respiration. Finally, antimycin A (2.5 μM) was added for nonmitochondrial respiration values records. The results were expressed as $O_2$ Flow per cell [pmol/(s*$10^6$ cells)].

### 2.6. LPS, Zonulin, IL-6, and TNF-α plasma/serum/intestine concentrations

Blood samples were collected in heparinized microtubes and centrifuged at 503 × g for 15 minutes using a refrigerated centrifuge (2–4°C) (Hettich, German) for plasma separation. To obtain the serum, blood samples (without heparin) remained at room temperature for 2 hours for clot formation, then were centrifuged at 503 × g for 15 minutes using a refrigerated centrifuge (Hettich). For homogenates, following the instructions of the respective kits, intestinal fragments (with no apparent presence of intestinal/fecal residues) were sonicated in 200 μL of LAL (LPS kit) or 500uL of sterile phosphate-buffered saline (PBS)(cat# D8537, Sigma) (Zonulin, IL-6, and TNF-α kits).

The LPS concentration was determined using the Limulus Amebocyte Lysate (LAL) QCL-1000 Endpoint Chromogenic kit (Lonza, Basel-SW). All endotoxin-free materials and reagents were purchased from the same supplier of the kit (Lonza, Basel-SW). The zonulin concentration was measured using the Elisa Mouse Zonulin (MBS748504-MyBioSource). The IL-6 and TNF-α concentration was assessed using the ELISA MAX Deluxe Set Mouse (cat# 431304 and cat# 430904, BioLegend· respectively). The absorbance measurements were performed in a microplate reader (Power Wave XS2, Biotek Inc., Winooski-US), at the wavelength of 405nm (LPS measurement) or 450nm (zonulin, IL-6, and TNF-α measurements).

The values were expressed as plasma or serum concentration in EU/mL for LPS, ng/mL for zonulin, and pg/mL for IL-6 and TNF-α.

For the intestinal concentration, the values were expressed as the ratio of the marker concentration obtained and the respective total protein concentration (μg/mL), previously measured in an aliquot of the respective homogenates using Bradford's reagent (Protein Assay Dye Reagent Concentrate, cat# 500-0006, Bio-Rad, Hercules-USA).

### 2.7. Intestinal permeability

The intestinal permeability was assessed using Lucifer Yellow (LY CH lithium salt, Invitrogen, cat# L453; MW 457.25 Da) as a paracellular tracer [58]. After a 6 h fast, the animals were anesthetized (with 80 mg/kg ketamine hydrochloride and 10 mg/kg xylazine hydrochloride, via intraperitoneal injection) and received by gavage LY solution (concentration of 100 μM in sterile saline, volume 7mL/kg body weight). After 1 h of the solution administration, they were euthanized, and the blood sample obtained was centrifuged at 8050 × g for 10 minutes at 4°C for separation of the plasma. In a 96-well microplate, 50 $\mu$L of the plasma samples were added to 50 $\mu$L of PBS (0.05M, pH = 7.4) (1:1 dilution). The reading was performed using a Fluorskan Ascent microplate reader (Thermo Scientific, USA), at a wavelength of 458 nm excitation and 535 nm emission. The values were expressed as LY plasma absorbance value by subtracting the blank value (plasma absorbance value of an animal that did not receive the marker by gavage).

### 2.8. Immunolabeling of tight junctional proteins and histone acetylation degree in intestine cryosections

The localization of the tight junctional proteins (claudins-2, -3, and ZO-1) and the degree of acetylation of histone (H3 and H4) in intestinal epithelia were determined by indirect immunofluorescence in cryosections of intestine fragments (jejunum, ileum, and colon) obtained from 12 h-fasted mice as previously described [31,58]. Briefly, intestine cryosections were incubated overnight at 4°C with the primary antibody (Supplementary Table S2; diluted in 3% BSA solution) and then, incubated with a FITC-conjugated specific secondary antibody (cat# F0382, Sigma; dilution 1:75 in BSA 1%) and DAPI (cat# D9542, Sigma; dilution 1:1000) for 2 h at room temperature. All sections were mounted on coverslips with ProLong Gold Antifade Mountant (Invitrogen cat# P36930) and photographed using a digital camera coupled to an inverted fluorescence microscope (Observer: Z1; Zeiss – AxioCam, MRC, Hamburg, Germany). Digital images of the intestine sections from all experimental groups were obtained and compared during the same session using identical microscope parameters (gain and time exposure). To determine the junctional content of each TJ protein, five images of intestinal epithelium were captured from each cryosection from animals from all experimental groups. Then, the integrated densities of 50 points per image, placed at the cell-cell contact region of enterocytes, were measured in all captured images using the free software ImageJ (given a total of 1,250 points sampled per experimental group for each TJ protein). To evaluate the degree of fluorescence of the different histones, five regions of the images were delimited, containing only nuclei of intestinal epithelial cells, and the degree of fluorescence and the delimited area was measured using the ImageJ program (http://rsbweb.nih.gov/ij/). The values were expressed as fluorescence intensity per area.

### 2.9. Immunoblotting of tight junctional proteins in intestine epithelial homogenates

Fragments of jejunum, ileum, and colon were collected, the epithelium scraped off using a scalpel, and then added to an antiprotease cocktail and sonicated. The epithelium homogenates were processed for immunoblotting using a standard protocol [58,59]. In addition, some of the jejunum homogenates were prepared to obtain Triton X-100-soluble (cytoplasmic) and Triton X-100-insoluble (junctional) fractions as described previously [60]. Briefly, epithelium homogenate aliquots (containing 50 μg of total proteins) were applied on 12% (claudin-2, -3) or 6.5% (ZO-1) polyacrylamide gels, and proteins were fractionated by electrophoresis, and electrophoretically transferred onto nitrocellulose membranes (Bio-Rad). After incubation overnight at 4°C with the primary antibody (Supplementary Table S3), the membranes were incubated with the specific secondary antibody conjugated with HRP (anti-rabbit IgG-HRP, cat# A4914, Sigma; dilution 1:600 in the basal solution containing 1% skimmed milk powder) for 2 h at room temperature. Immunoreactive bands were detected using an enhanced chemiluminescence kit (Super Signal, Thermo Fisher Scientific, USA) and an imaging system (Genome Gene, Syngene Bio Imaging, UK). The relative size of the immunoreactive bands was quantified by densitometry using the ImageJ software. The same membranes were incubated with an anti-beta-actin antibody, used as an internal control. Optical densitometric values were expressed as a ratio of the respective proteins and beta-actin signals. In the case of lack of signal for beta-actin after membrane reblotting, the TJ protein band densitometry was normalized by the total protein loading revealed by the membrane previously stained with Ponceau.

### 2.10. Quantitative real-time PCR for Claudins-1 -2, -3, Occludin, and ZO-1 genes in homogenates of intestine fragments

Fragments of jejunum, ileum, and colon were collected, the epithelium scraped off using a scalpel, and prepared for RNA extraction using the TRIzol Reagent (cat# 15596018; Invitrogen, Carlsbad, CA; 1 mL of Trizol per 100 mg of tissue), homogenized with polypropylene pestles (Axygen Tissue Grinder) in 1.5 mL centrifuge tubes. To each 1 mL of Trizol was added 0.2 mL volume of chloroform for precipitation (according to the TRIzol Reagent manufacturer's recommendations). cDNA synthesis was performed from 0.5 $\mu$g RNA samples of each fragment using High-Capacity cDNA Reverse Transcription Kit (Applied Biosystems, Foster City, CA, USA). The primers for *Claudins-1, -2, -3, Occludin*, and *ZO-1*, and the housekeeping *Actb1, Gapdh,* and *Rps29* genes were designed and tested against the *Mus musculus* genome (GenBank) (Supplementary Table S4). The absolute quantities of target transcripts were normalized against the endogenous *Actb1* control, which proved to be the best internal control for the experimental conditions tested using Bestkeeper for comparison with *Gapdh* and *Rps29* (data not shown). Analysis of gene expression was done by absolute quantification of mRNAs as previously described [61]. The reactions were performed in cDNA samples (500 ng/$\mu$L), with the SYBR Green method (ABI Fast SYBR Green Master Mix, cat# 4385612), using the Applied Biosystems 7,500 Real-Time PCR Systems (Applied Biosystems, Foster City, CA, USA).

### 2.11. Caco-2 cell culture and treatments

Caco-2 cells (human colorectal adenocarcinoma) were cultured in Eagle medium modified by Dulbecco (high glucose) (DMEM), supplemented with 10% fetal bovine serum, 2% nonessential amino acids, 1% L-glutamine and 60 mg/L of gentamicin, and kept in a humidified incubator at 37°C with 5% $CO_2$ (Incusafe Sanyo MCO-17A, Sanyo Electric Ltd., Japan). The medium was changed at least three times a week and the passages were performed by partial digestion with a trypsin/EDTA solution. Before cell seeding, cell culture inserts containing a membrane with a diameter of 12 or 30

mm (Millicell, Merck Millipore, German) were coated with collagen solution extracted from the Wistar rat tails [62]. Then cells were seeded at a density of 1.5 × $10^4$ cells/cm². After total confluence (approximately 10–11 days), the monolayers were exposed on both sides (apical + basal) to the luminal content of the small intestine obtained from mice of the different experimental groups (*i.e.*, C, CB, HF, HFB). For that, mice from C, CB, HF, and HFB groups were euthanized, the small intestine removed under sterile conditions (within the laminar flow), and the luminal contents washed with 15 mL of sterile Krebs-bicarbonate buffer (concentration in mM: NaCl 115, KCl 5, $MgCl_2$ 1, $CaCl_2$ 1.24, $NaHCO_3$ 1, HEPES 15; pH = 7.4 equilibrated with 5% $CO_2$) containing 100 mg/dL of glucose. The small intestinal segment was chosen to obtain the luminal content for *in vitro* exposure since, in previous work [41], we have shown that the luminal content of the small intestine had a greater disruptive effect on the intestinal epithelial barrier, even at short period (6 h) than that from the large intestine. The solution obtained by washing the intestinal luminal content was centrifuged in Falcon tubes at 2,100 × g for 90 seconds, and the supernatant was collected and diluted 1:5 ratio in sterile Krebs-bicarbonate. This dilution of the intestinal contents of the small intestine was necessary to eliminate/decrease the cytotoxic action on cells, as noted and described previously [41]. Then, cell monolayers were exposed to the intestinal suspensions for 6 h on both apical and basal surfaces.

### *2.12. Transepithelial electrical resistance (TEER) and paracellular flux across Caco-2 cells*

The TEER measurement was performed using two Ag/AgCl 'chopstick' electrodes coupled to a combined voltmeter and a constant current source (EVOM, World Precision Instruments, UK). TEER was measured every hour during the 6 h interval after cell exposure to the intestinal luminal content. The final TEER was calculated as follows: the resistance of the blank membrane insert (without cells) was subtracted from the gross TEER value across Caco-2 monolayers and then multiplied by the membrane area (1.13 $cm^2$) to obtain the final TEER value (·Ω.cm²). The TEER data were depicted in the graph as a percentage of the initial mean value (at 0 h, before exposure to luminal content).

To assess the paracellular permeability across Caco-2 monolayers, cells (cultured on 30 mm permeable culture inserts) were transferred to a new plate containing the suspension of intestinal luminal content (from the different experimental groups), or Krebs' solution, where the paracellular marker Lucifer Yellow (MW 457.25 Da) was added only to the basal solution at the final concentration of 100 μM. In the apical environment, an identical solution was added, but without LY. After the incubation period (6h), samples of the apical and basolateral solutions were collected. The samples were read in triplicate (0.2mL) on a 96-well plate using the Synergy H1 microplate reader (Biotek Instruments, USA) at 428 nm (excitation wavelength) and 535 nm (emission wavelength). The transepithelial flux of LY (Ft), taken as an index of paracellular permeability, was calculated as follows: Ft = Apical fluorescence × 100/Apical fluorescence + Basal fluorescence.

### *2.13. Immunofluorescence and immunoblotting for junctional proteins in Caco-2 monolayers*

Caco-2 monolayers were fixed and maintained in methanol at −20°C until the indirect immunofluorescence reaction. After washing with PBS, the monolayers were incubated with 3% fetal bovine serum (FBS) in PBS for 30 min at room temperature and then incubated with the primary anti-Claudin-1 (Abcam ab15098, 1:30) or anti- ZO-1 (Invitrogen 7300, 1:50) antibodies diluted in PBS plus 3% FBS, overnight at 4°C. Subsequently, the monolayers were incubated for 1 h with the FITC-conjugated specific secondary antibody FITC (Sigma- F0382, 1:75) and DAPI (Sigma, cat# D9542) (dilution 1: 1000 in PBS plus 3% FBS) at room temperature. The monolayers were washed five times with PBS, mounted on coverslips with ProLong Gold Antifade Mountant, and photographed using a digital camera coupled to an inverted fluorescence microscope (Observer.Z1; Zeiss – AxioCam, MRC, Hamburg. Germany) at the same microscopic session, using the same gain/contrast parameters to compare the fluorescence degree between the treated and control groups.

For immunoblotting, Caco-2 monolayers were scraped from the 30 mm tissue inserts using a cell scraper and added to 1 mL of PBS. After centrifugation at 126 × g, the supernatant was discarded, and the cell pellet was resuspended in 20 μL of antiprotease cocktail and then sonicated [41]. Aliquots containing an equal amount of total proteins (20 μg) were processed for immunoblotting as described above for intestine homogenates. The membranes obtained were incubated sequentially overnight at 4°C with the primary antibody (Supplementary Table S5) and then with the specific secondary antibody conjugated with horseradish peroxidase (HRP-A4914-Sigma-1:600) for 2 h at room temperature. The immunoreactive bands were detected using the enhanced Super Signal chemiluminescence kit, the immunoreactive bands were quantified by densitometry, and expressed as a ratio of the respective proteins and beta-actin signals, as previously described [41].

### *2.14. Statistical analysis*

To determine the degree of statistical significance among the four experimental groups, we have used the One-way ANOVA, followed by the Bonferroni *post hoc* test to compare selected pairs of data. Two-way ANOVA, followed by the Bonferroni post hoc test, was used to statistically analyze the GTT curve data. Results were expressed as means + SEM (Standard Error of the mean), and the significance level was set at $P < .05$. All statistical analyses were performed using GraphPad Prism Version 5.00 for Windows (GraphPad Software, USA).

## 3. Results and Discussion

### *3.1. Supplementation with sodium butyrate restores energy metabolism compromised by a high-fat diet in prediabetic mice*

SCFAs are being studied as possible interventions for the prevention of metabolic disorders such as obesity and T2D due to their involvement in several signaling pathways influencing cell metabolism and inflammation [26,27,63]. Interestingly, the formation of SCFAs, particularly butyrate, is reduced after the ingestion of high-fat diets [64], while dietary supplementation with butyrate can inhibit some of the metabolic dysfunctions in diabetic animals [22,25–29,31].

In the present work, we focused on the beneficial effect of butyrate on metabolism and intestinal barrier at the early stages of T2D using an animal model of prediabetes that has been previously well-characterized [31,47,48,59]. Our mice display body/metabolic changes typical of type 2 prediabetes (*i.e.*, increased body weight/adiposity, insulin resistance, moderate hyperglycemia, significant hyperinsulinemia associated with compensatory beta-cell hyperplasia) [41,47,48,65], besides showing impaired intestinal barrier that was not accompanied by endotoxemia and local/systemic inflammation [58,59]. This model gives a unique possibility to investigate the effect of butyrate on metabolism during type 2 prediabetes not accompanied by an evident inflammatory state, which has not been directly explored by others

[22,25,28,29,31]. Also, we included the control and control butyrate groups to allow us to assess the systemic effect of this SCFA *per se* (*i.e.*, in the absence of the metabolic challenges provided by HF diet feeding) that has been scarcely examined.

As shown in Fig. 1, exposure to HF diet for 60 days increased fasting glycemia (Fig. 1a) and led to glucose intolerance as assessed by GTT (Fig. 1b and c). HF-fed mice also displayed dyslipidemia characterized by significant increased plasma levels of triglycerides (+78%) (Fig. 1d), cholesterol (+50%) (Fig. 1e), and low-density lipoprotein cholesterol (LDL) (+72%) (Fig. 1f), but not of low high-density lipoprotein cholesterol (HDL) (Fig. 1g) as compared to the control group. Sodium butyrate had a marked effect on fasting glycemia and glucose tolerance, improving both parameters in the prediabetic mice treated with butyrate (HFB) in relation to the HF group (Fig. 1a-c). This SCFA did not significantly alter cholesterol, TG, and LDL levels in the HF-fed groups (HFB *vs* HF) (Fig. 1d-f). Nevertheless, the HFB group seems to display a small decrease in TG and LDL parameters in comparison with the HF group (−14.1% TG; −13.9% LDL), which resulted in a nonsignificant difference with its respective control (CB *vs* HFB). Yet, sodium butyrate *per se* did not change the serum concentration of glucose and lipids in animals fed a chow diet (CB *vs* C) (Fig. 1a-g).

These effects of butyrate seen herein are in line with our previous study [31], which demonstrated that dietary supplementation with butyrate had a beneficial effect on glucose homeostasis and peripheral insulin sensitivity. All these alterations occurred without significant changes in daily food consumption or energy intake, as shown previously [31], suggesting a direct effect of butyrate on glucose metabolism. As shown in Fig. 1h, qPCR analysis in the hypothalamus from the groups receiving butyrate supplementation (CB and HFB) showed no significant differences in anorexigenic (*Cart, Pomc*) and orexigenic (*Npy, Agrp*) markers [66] when compared to their respective controls (C and HF), confirming that butyrate does not affect food intake in our animal model as reported before [31].

To investigate the mechanism through which butyrate protects from HF diet-induced dysregulation of carbohydrate metabolism during prediabetes, we assessed basal energy expenditure. The group receiving a HF diet showed a decrease in EE ($P < .05$) (Fig. 1i), oxygen consumption ($VO_2$) ($P < .05$) (Fig. 1j), and respiratory quotient (RQ) ($P < .001$) (Fig. 1k) compared to the control group during the night cycle. The group receiving the high-fat diet with supplementation with 5% sodium butyrate (HFB) showed an increase in EE ($P < .05$) (Fig. 1i) and $VO_2$ ($P < .05$) (Fig. 1j) when compared to the HF diet group, reaching levels similar to the C and CB groups. However, butyrate did not affect the RQ (Fig. 1k). As shown in Fig, 1l, sodium butyrate (in CB and HFB groups) did not significantly affect motor activity in comparison with the groups that did not receive supplementation (C and HF). Again, the effects of butyrate were exclusive to mice on a HF diet (Fig. 1i-l).

Taken altogether, butyrate significantly reversed the decrease in EE and $VO_2$ observed in our prediabetic mice, restoring these parameters to control levels, without affecting motor activity. Gao et al. [25] also reported the beneficial effect of butyrate supplementation on EE changes induced by eating HF diet, though this effect was not observed by others [30,67]. This discrepancy concerning butyrate actions may be explained by differences in the metabolic state, diet composition, and exposure among the different animal models employed by these studies.

Interestingly, our prediabetic mice that received butyrate displayed a RQ level as well as a lipid profile that was similar to that of mice fed only the HF diet. The RQ is the ratio of carbon dioxide production to oxygen consumption and reflects the relative contribution of fat, carbohydrate, and protein to fuel oxidation [68]. Our HF diet-treated animals (HF and HFB) displayed a RQ of 0.85 (in contrast to the RQ of 0.95 in C and CB groups), indicating a preference for fat over carbohydrate oxidation, which was not affected by the butyrate administration. These data suggest that butyrate displays a relatively small effect on circulating lipids in HF diet-fed prediabetic mice, and it does not alter fat oxidation in these animals. This contrasts with the marked protective action of butyrate on glucose homeostasis seen herein. Although we do not have a conclusive explanation for this observation, it is plausible to suggest that butyrate does not reduce the intestinal absorption of lipids, and, by doing so, the circulating lipids remain at high levels under HF diet ingestion that cannot be counteracted by the metabolic actions of butyrate, at least at the early stage of T2D. Consistent with this idea, it has been demonstrated that dietary fat digestion and absorption in the gastrointestinal tract are identical between HF diet-fed mice that received butyrate supplementation and those that did not [25].

We next investigated the potential effect of butyrate on adipose tissue depot at the early stages of T2D. As shown in Fig. 2, exposure to HF-diet resulted in an increase in total body weight gain (+438%) (Fig. 2a), and the weight of both eWAT (+328%) (Fig. 2b) and rWAT (+457%) (Fig. 2c) as compared to C group. As revealed by microtomography, increased fat mass (+253%) (Fig. 2d) and decreased lean mass (−37%) were also observed in prediabetic animals in comparison with the C group (Fig. 2e), resulting in an overall increase in fat/lean mass ratio (+459%). Dietary supplementation with 5% sodium butyrate (HFB) reduced body weight gain (−46%) (Fig. 2a), rWAT mass (−26%) (Fig. 2c), and fat/lean mass ratio (−38%) (Fig. 2d,e,f), but it did not change eWAT depot weight (Fig. 2b) when compared to the HF group. Sodium butyrate (CB) did not affect these parameters in chow diet-fed mice (Fig. 2a-f).

An increase in fat-to-lean mass ratio (*i.e.*, increased body fat depot associated with a reduction in muscle mass) is a good predictive indicator of insulin resistance and prediabetes, as well as metabolic syndrome and cardiovascular risks [69–71]. Micro-CT imaging revealed a marked inhibition of fat mass gain after butyrate treatment (Fig. 2f), which was associated with a significant increase in lean mass leading to an improvement of the fat-to-lean mass ratio in these prediabetic animals. Interestingly, the effect of butyrate on adiposity seemed to be dependent on the type of adipose depot, promoting a more significant reduction of the rWAT as compared to the eWAT in prediabetic mice. This agrees with the observation that each WAT depot has specific morphofunctional characteristics and displays a differential response to caloric restriction, being the rWAT more responsive than the eWAT [72].

A possible contributing factor to the anti-diabetogenic and anti-obesogenic effects of butyrate is its protective action on BAT [22,30]. Due to the high expression of *Ucp-1*, BAT uncouples substrate oxidation from ATP production by generating a process called nonshivering thermogenesis [7,73]. BAT activity has been inversely associated with adiposity and indexes of metabolic disorders suggesting that increasing BAT mass and/or activity may be a target for pharmacologic and nutritional interventions that modulate EE to treat obesity and T2D [7,74]. HF diet induced “whitening” of iBAT as revealed by the increase in intracellular lipid accumulation, as confirmed morphometrically ($P < .0001$) (Fig. 2g and h), increased iBAT weight ($P < .0001$) (Fig. 2i) and decreased *Ucp1* mRNA levels ($P < .05$) (Fig. 2j); butyrate significantly attenuated these changes but did not affect these parameters in control lean mice (CB *vs* C groups) (Fig. 2g-j). The decreased *Ucp1* mRNA level in our prediabetic mice is consistent with the lower EE displayed by these animals, as well as the increase in lipid accumulation seen in BAT. The data show that supplementation with butyrate preserved the histological characteristics of brown adipose tissue, as well as restored the tissue expression of *Ucp1* to control levels in HF diet-fed mice.

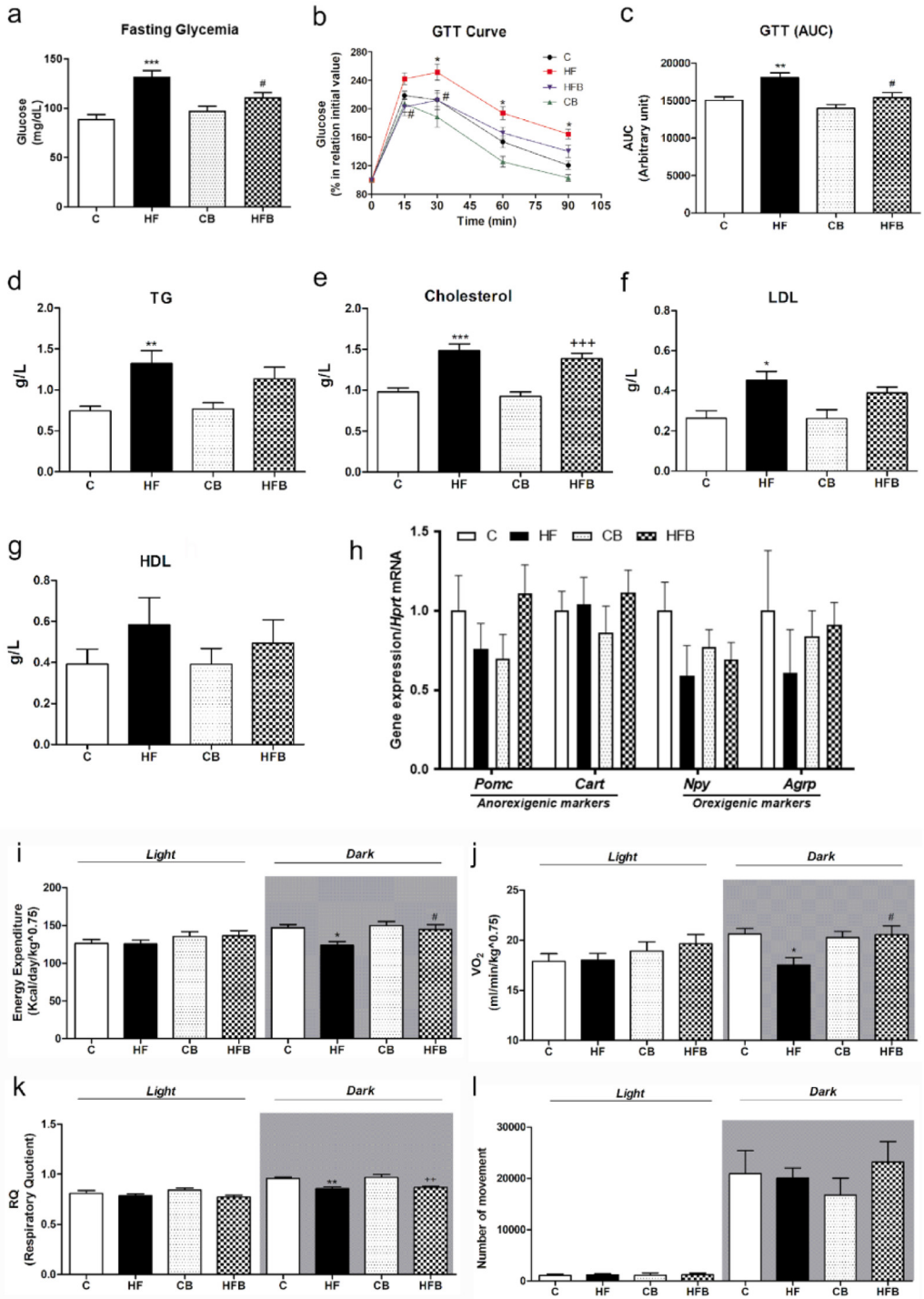


**Fig. 1.** Effect of butyrate on glucose metabolism (a-c), lipidemia (d-g), hypothalamic expression of orexigenic/anorexigenic genes (h), and basal metabolism (i-l) in prediabetic mice. In comparison with the control group, the high-fat diet (HF) induced a significant intolerance to glucose as assessed by the Glucose Tolerance Test (GTT) curve in b, the area under the curve (AUC) in c associated with a significant increase in fasting glycemia (a), in the level of the triglycerides (TG) (d), cholesterol (e), and LDL fraction (f) but no significant changes in HDL level and gene expression in the hypothalamus related to food intake (h). Dietary supplementation with 5% sodium butyrate presented a protective effect by restoring the glucose homeostasis (a-c), but only partially inhibited dyslipidemia (d-f) induced by the HF diet (HF group) and had no effect on orexigenic/anorexigenic gene expression in the hypothalamus (h). Also, high-fat diet group showed a significant decrease in Energy Expenditure (EE) (i), Oxygen Volume (VO2) (j), and Respiratory Quotient (RQ) (k) at the nocturnal period. The diet supplementation with butyrate in the HFB group significantly reversed the changes in EE and $VO_2$ induced by HF diet (i and j) but did not affect the RQ values (k). No difference in motor activity during day and night was observed among the experimental groups (L). Butyrate supplementation alone (CB) did not affect the evaluated parameters when compared to the control group (C) (a-l). Data in a-l are expressed as means + SEM ($n$ = 6–15 mice/group, 2–4 independent experiments). Groups: C: control (fed a regular diet alone); HF: high-fat diet alone; CB: Control+butyrate; HFB, high-fat diet+butyrate. $^{*}P < .05$, $^{**}P < .001$, $^{***}P < .0001$ compared to C group; $\#P < .05$ compared to HF group; $++P < .005$, $+++P < .0001$ in relation to CB (one-way ANOVA followed by Bonferroni's post-test for all data except the GTT curve (b) that was analyzed by two-way ANOVA followed by Bonferroni's post-test).

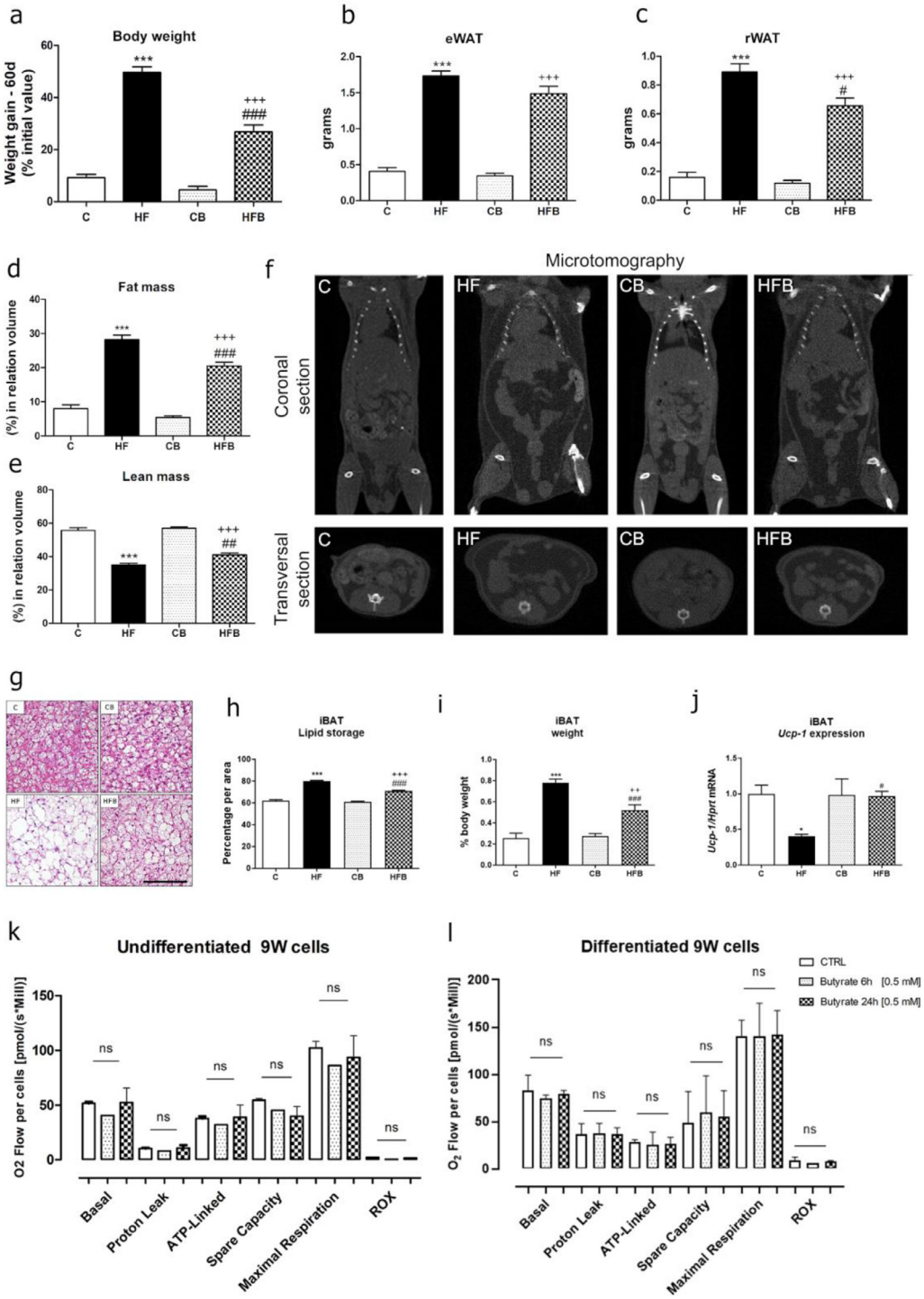


**Fig. 2.** Effect of butyrate on body weight (a), fat/lean mass (b-f), and brow adipose tissue (g-l) in prediabetic mice. The fat depot was assessed by the weight of epididymal (eWAT) (b) and retroperitoneal white adipose tissue (rWAT) (c), expressed as grams. The intake of a high-fat diet induced a significant increase in body weight gain (a), eWAT (b), rWAT (c), and fat mass (d) associated with a significant decrease in lean mass (d)(d and e determined by microtomography). In f, representative tomography images of mice from each experimental group. Dietary supplementation with butyrate partially reversed these alterations in the HFB group (a-f) but did not display an effect *per se* in the CB group. Data in a-e are expressed as means + SEM ($n$ = 11–19 mice/group, 2–6 independent experiments). In g, representative photomicrographs of interscapular brown adipose tissue (iBAT) histological sections stained with HE of each experimental group. Scale bar, 50μm. In comparison with the control group, the HF diet induced an increase in the intracellular lipid storage (g and h) and weight (i) associated with a decrease in *Ucp-1* expression (j), indicative of "whitening" of iBAT. All these changes in iBAT were significantly inhibited by dietary supplementation with 5% sodium butyrate (HFB group) (g-j). The *Ucp-1* expression was determined in iBAT homogenates by qPCR (j). *In vitro* experiments, assessing cellular bioenergetics in undifferentiated (k) and differentiated (l) 9W cells, showed no significant (*ns*) changes after 0.5 mM butyrate exposure. Data in h-l are expressed as means + SEM (h-j, $n$ = 5–8 mice/group, 2 independent experiments; k-l, $n$ = 3–4 cell monolayers, two independent experiments). Groups: C, control (fed a regular diet alone); CB, Control+butyrate; HF, high-fat diet alone; HFB, high-fat diet+butyrate. $^{*}P < .05$, $^{***}P < .0001$ compared to C group. $\#P < .05$, $\#\#P < .001$, $\#\#\#P < .0001$ compared to HF group, $++P < .001$, $+++P < .0001$ compared to CB group (one-way ANOVA followed by Bonferroni's post-test).

Since sodium butyrate increased EE and restored BAT morpho-functional characteristics *in vivo* after HF diet intake, we investigated whether it could have a direct effect on the bioenergetics of preadipocytes *in vitro*. For this, we used a murine white subcutaneous adipocyte precursor cell line, 9W, with the potential to differentiate into *Ucp1*-positive adipocytes [53]. The *in vitro* experiments performed herein were designed to evaluate whether butyrate has a cell-autonomous effect on *Ucp1*-expressing adipocytes. As shown in Fig. 2k and l, the addition of butyrate at 0.5mM concentration to the cell media for 6 h and 24 h did not affect the oxygen consumption by cultured 9W cells in any of the experimental conditions tested, besides showing no cytotoxic effect (viability after 24 h exposure to 0.5mM: Control 9W cells 100%; undifferentiated 9W cells 101.2 ± 6.6 (4) %; differentiated 9W cells 95.6 ± 6.6 (4) %). It is noteworthy that this work used a concentration of 0.5 mM sodium butyrate that was not toxic for this cell type and is well above the physiological concentration range in humans [27,75], and HF-fed rodents [76]. Therefore, the effect on EE observed *in vivo* with sodium butyrate supplementation was not seen in our *in vitro* system. Despite the limitation of using cultured adipocytes as an indicator of *in vivo* metabolic alterations in adipose depots, these preliminary data suggest that butyrate does not have a direct effect on *Ucp1*-positive adipocytes. This finding reinforces the idea suggested by others [7,30] that the mechanism of action of butyrate may be systemic and involve neural circuits or other body regulatory pathways of BAT function.

### *3.2. Sodium butyrate reverses the disruption of the intestinal epithelial barrier through membrane trafficking of TJ proteins in prediabetic mice*

In the next step of this work, we investigated whether the beneficial effect of butyrate on metabolism is associated with actions on intestinal permeability in our type 2 prediabetes animal model. Previous data already indicated that butyrate has a protective effect on the intestinal barrier, as this SCFA decreased intestinal permeability to FITC-Dextran in CB and HFB groups as compared to the C group, as well as inhibited the redistribution of claudin-1 in the intestinal epithelium in prediabetic animal [31]. Fig. 3 shows the intestinal permeability to the LY marker in the different experimental groups studied (C, HF, CB, and HFB). The reason for using LY here was based on our previous work indicating that this molecule constituted a more adequate marker for the assessment of intestinal permeability *in vivo* than FITC-Dextran [58,59]. These studies demonstrated that the prediabetes state in our animal model involves selective regulation of the permeability of the paracellular barrier, favoring the transepithelial transport of small molecules (such as LY) rather than of large molecules (with an MW> 4,000) such as FITC-Dextran. The increase of paracellular transport to small molecules is often associated with modulation of the TJ permeability [59,77] rather than being involved with general damage to the integrity of the epithelium [43,78]. In accordance with these results, we observed here an increase in the plasma concentration of the LY marker in mice that were fed a high-fat diet (HF group) ($P < .0001$) compared to the control group (C), which indicates an increase in intestinal permeability for this marker in the prediabetic mice (Fig. 3). Supplementation with sodium butyrate reduced the presence of this marker in the plasma ($P < .0001$) in mice from the HFB group compared to the HF group. Also, there was no difference in intestinal permeability to LY between mice that received a standard diet with butyrate (CB) compared to the group that received a standard diet without butyrate (C), which reinforces the idea that butyrate has its biological effect manifested mainly in conditions of metabolic dysfunction, such as after the administration of a HF diet.

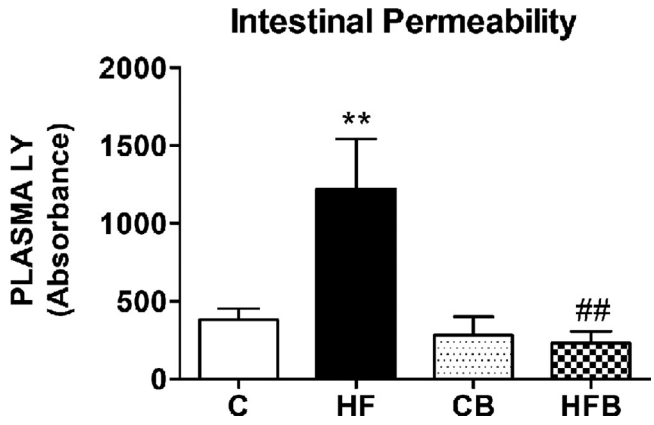


**Fig. 3.** Dietary supplementation with sodium butyrate inhibits the increase in intestinal permeability to the paracellular marker, Lucifer Yellow (LY), in prediabetic mice. Sodium butyrate restored intestinal permeability in HF diet-fed prediabetic mice (HFB), while butyrate *per se* (CB) maintained these parameters at the level of the control group (C). The values represent the means + SEM. ($n$ = 10–12 animals/group, 4 independent experiments). Groups: C, control (fed a regular diet alone); CB, Control+butyrate; HF, high-fat diet alone; HFB, high-fat diet+butyrate. $^{**}P < .001$ compared to C group; $\#\#P < .001$ compared to the HF group (one-way ANOVA followed by Bonferroni's post-test).

Following the idea that sodium butyrate has a positive effect on the intestinal epithelial barrier confirmed here by the paracellular permeability test, we have investigated the structural integrity of the intestinal epithelial barrier by immunodetection of proteins associated with TJ (claudin-2, -3, and ZO-1) in cryosections of fragments of the small intestine (jejunum and ileum) and large intestine (colon). As shown in Figs. 4–6, exposure to HF-diet resulted in significant changes in the junctional content of these proteins in the intestinal epithelium, which included a significant decrease in the intercellular labeling of claudin-2 (Fig. 4e and j), claudin-3 (Fig. 5e and j), and ZO-1 (Fig. 6e and j) in both jejunum and ileum ($P < .0001$), while, in the colon, we observed a decrease of claudin-3 (Fig. 5o) in association with an increase in junctional content of claudin-2 (Fig. 4o) and ZO-1 (Fig. 6o) ($P < .0001$), which were consistent with data previously reported by our group [58,59]. These changes indicate significant disorganization of TJ structure in the intestinal epithelium of prediabetic mice, which certainly can have a functional impact on the intestinal barrier properties [16,79]. In particular, the reduction in the junctional content of the well-known barrier-forming claudins, Cld-1, as reported previously [31], and Cld-3, suggests a rupture of the intestinal epithelial barrier allowing the passage of molecules, which agrees with the data obtained from intestinal permeability to LY in HF-diet fed prediabetic animals.

Interestingly, sodium butyrate supplementation (HFB group) completely reversed or significantly inhibited these alterations in the TJ junctional content in intestinal epithelial cells, as assessed by immunofluorescence, except for the ZO-1 protein in the colon, when compared to the HF group (Fig. 4–6). Also, in comparison with the CB group, the HFB group showed a further increase in the ZO-1 ($P < .0001$ jejunum, Fig. 6c, d, e; $P < .05$ ileum, Fig. 6h, i, j), and in claudin-3 junctional contents ($P < .0001$ in the ileum, Fig. 5h, i, j, and colon, Fig. 5m, n, o), suggesting a greater reinforcement of the TJ-mediated paracellular barrier when butyrate was administered in conjunction with the HF diet. Yet, the CB group showed no significant change in the junctional content of TJ proteins (Cld-2, -3, and ZO-1) in any of the intestinal segments studied (jejunum, ileum, and colon) when compared to the C group (Fig. 4–6), suggesting that butyrate has no effect *per se* on the intestinal paracellular barrier.

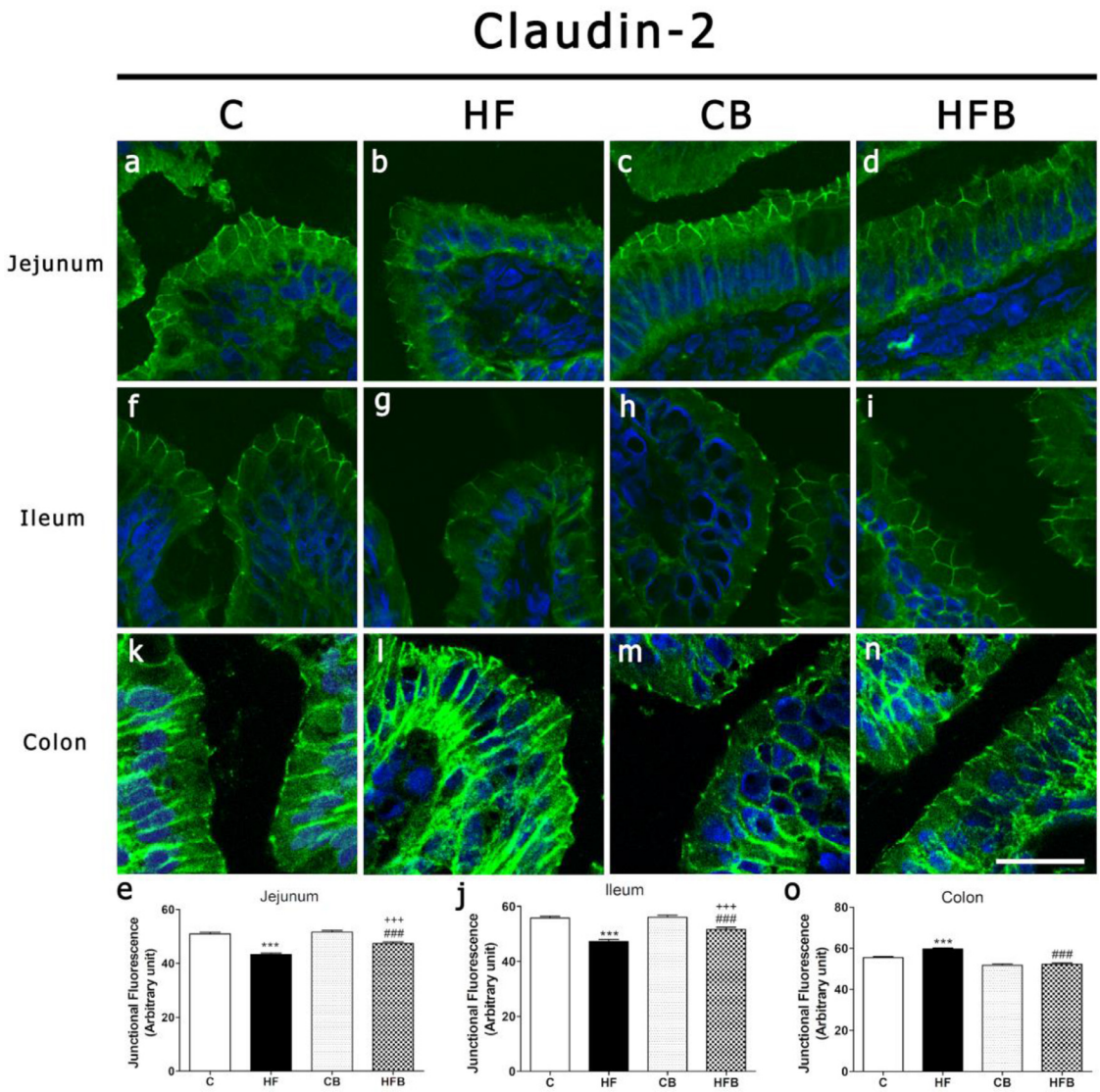


**Fig. 4.** Effect of the dietary supplementation with sodium butyrate on the cellular distribution of Claudin-2 (Cld-2) in the epithelium of small intestine (jejunum and ileum) and large intestine (colon) of mice fed a standard or high-fat (HF) diet. Images show the immunofluorescence detection of Cld-2 (in green; DAPI/nuclei in blue) in cryosections of intestine segments of mice from the different experimental groups (C/Control, HF/High-fat diet, CB/Control+Butyrate, and HFB/High-fat diet+Butyrate). The analysis of the degree of fluorescence at the cell-cell contact showed that HF diet induced a significant reduction of the Cld-2 content at the intercellular region of the epithelial cells of the jejunum (e) and ileum (j) but led to an increase in the junctional content of this protein in the colon epithelium (o). Butyrate supplementation partially reversed the effects of the HF diet on the junctional content of this TJ protein in the three intestinal segments studied (e, j, o). Bar, 25 $\mu$m. The values of the degree of junctional fluorescence represent the means + SEM (5 animals/group, 2–4 independent experiments). $^{***}P < .0001$ compared to C group; $^{###}P < .0001$ compared to HF group; $^{+++}P < .0001$ compared to CB group (one-way ANOVA followed by Bonferroni's post-test).

The regulation of the TJ structure/function may occur through alteration in the expression of TJ genes, in the protein amount, and/or cellular redistribution of its structural proteins, which can involve epigenetic regulation, changes in the turnover process, or post-translational modifications such as phosphorylation/dephosphorylation, palmitoylation and/or ubiquitination [80–84]. Another possibility of modulating the selective permeability of the TJ is through the interaction between its main constitutive proteins, the claudins that can be barrier-forming (*e.g.*: Cld -1, -3, -4, -5, -8) or pore-forming (*e.g.*: Cld -2, -7, -12) proteins [17,18,85].

The supplementation with sodium butyrate reversed or significantly inhibited the effects of the HF-diet on the organization of proteins at TJ site in the intestinal epithelia of prediabetic mice. Since butyrate is a well-known inhibitor of HDAC causing histone hyperacetylation, it can potentially facilitate or increase the cell expression of certain genes [22,23,36,86]. To investigate whether butyrate has an epigenetic effect on enterocytes of prediabetic mice, we assessed the levels of acetylated histones H3 and H4 in cryosections of the intestinal segments (jejunum, ileum, and colon) by indirect immunofluorescence. As shown in Fig. 7, no significant changes were observed in the nuclear levels of acetylated histones in the intestinal epithelium from the different experimental groups, except in the case of acetylated H3 histone which showed a significant increase in its immunodetection in the colon of HFB mice compared to the C group (Fig. 7d). These results point to an absence or a subtle epigenetic action of butyrate on enterocytes depending on the intestine segment in our animal model. Corroborating these data, the positive effect of butyrate on the TJ structure was not associated with changes in TJ protein expression, as assessed by Western Blot (Fig. 8a and Figure S1 (Supplementary

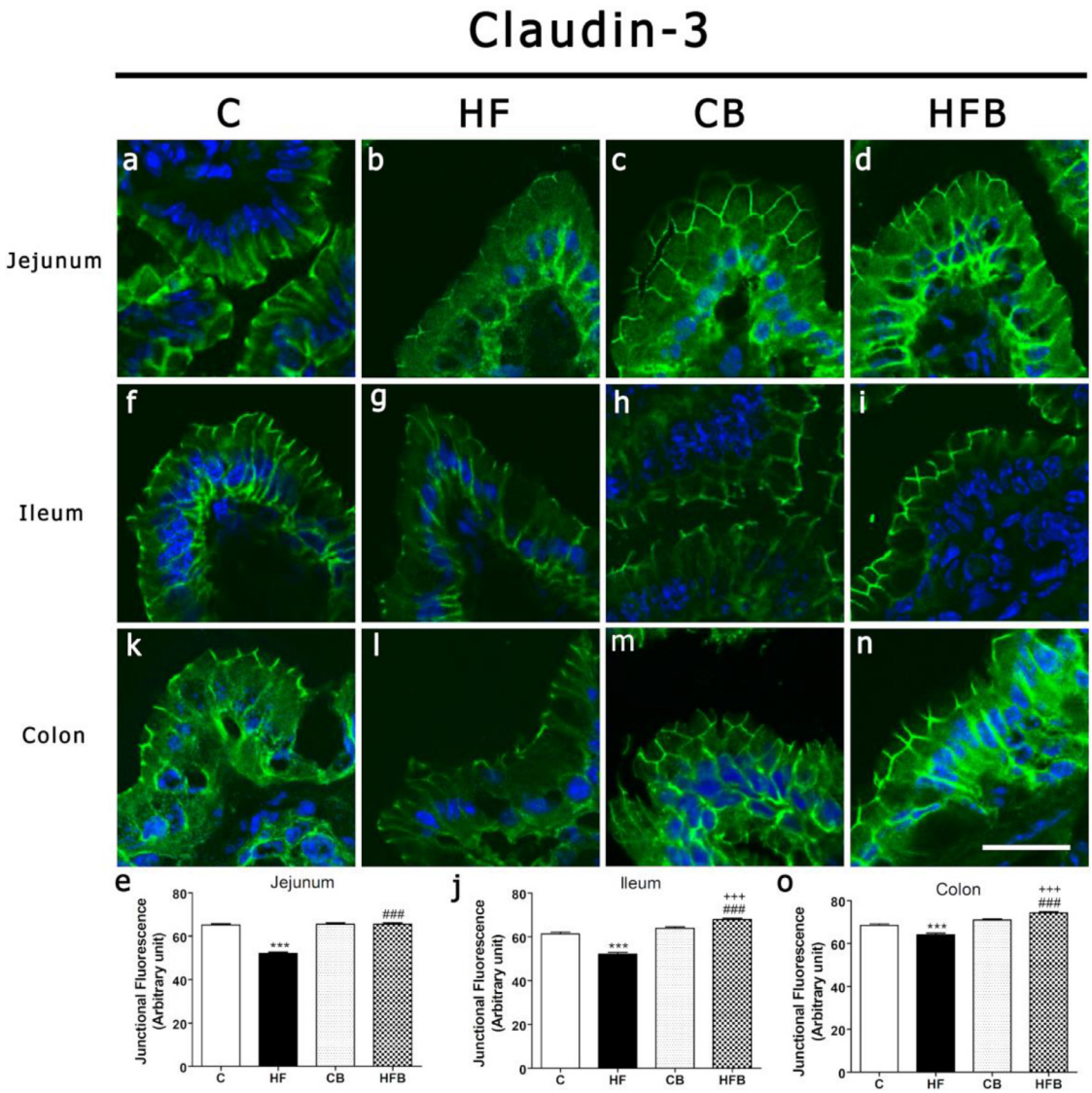


**Fig. 5.** Effect of the dietary supplementation with sodium butyrate on the cellular distribution of Claudin-3 (Cld-3) in the epithelium of small intestine (jejunum and ileum) and large intestine (colon) of mice fed a standard or high-fat (HF) diet. Images show the immunofluorescence detection of Cld-3 (in green; DAPI/nuclei in blue) in cryosections of intestine segments of mice from the different experimental groups (C/Control, HF/High-fat diet, CB/Control+Butyrate, and HFB/High-fat diet+Butyrate). The analysis of the degree of fluorescence at the cell-cell contact showed that Cld-3 immunostaining at the intercellular region of the intestinal epithelium was significantly reduced in all the intestinal segments studied (jejunum-e, ileum-j, and colon-o) in mice after HF diet. The supplementation with sodium butyrate significantly reversed this effect in the HFB group as compared to HF mice and even increased the Cld-3 immunoreaction in the ileum (j) and colon (o) when compared to the CB group. Bar, 25 $\mu$m. The values of the degree of junctional fluorescence represent the means + SEM (5 animals/group, 4 independent experiments). $^{***}P < .0001$ compared to C group; $\#\#\#P < .0001$ compared to HF group; $+++P < .0001$ compared to CB group (one-way ANOVA followed by Bonferroni's post-test).

Material)) or gene expression as assessed by qPCR (Fig. 8b and Figure S2 (Supplementary Material)).

To determine whether butyrate treatment affects the cellular distribution and the specific amount of the protein fraction associated with the TJ [60,84], we further analyzed the changes in the amount of claudin-3 in detergent-soluble (cytosolic or loosely associated with membrane) and detergent-insoluble (representing protein incorporated in the TJ) fractions in jejunum fragments of mice from the different experimental groups (Fig. 8c). Following the rationale of our work, claudin-3 was chosen since it participates directly in the formation of the paracellular barrier structure ("gate") to ions and molecules [17,18]. Therefore, Cld-3 seems to be the appropriate marker to investigate the possible effect of butyrate on the cellular trafficking of a TJ barrier-forming protein. Our data on immunoblotting for the soluble (S)(cytoplasmic) and insoluble (I)(junctional) fractions of jejunum homogenates show a relative increase in the translocation of claudin-3 from the cytoplasm to the TJ region after supplementation with butyrate (CB and HFB *vs* C and HF) (Fig. 8c), that was statistically significant in the case of HFB group ($^{*}P < .05$, HFB-I *vs* HFB-S). Also, the result in Fig. 8c showing a higher content of Cld-3 in the junctional fraction in HFB-I in comparison with HF-I ($\#P < .05$) agrees with the immunofluorescence findings depicted in Fig. 5e, which also shows higher junctional immunolabeling for Cld-3 in jejunum epithelial cells after butyrate in mice fed a HF diet (Fig. 5d HFB *vs* Fig. 5b HF). Therefore, our data suggest that butyrate has an action on the intestinal barrier *in vivo* by probably inducing the trafficking of junctional proteins from their cytoplasmic pools to the TJ region at cell-cell contact, reinforcing the paracellular barrier.

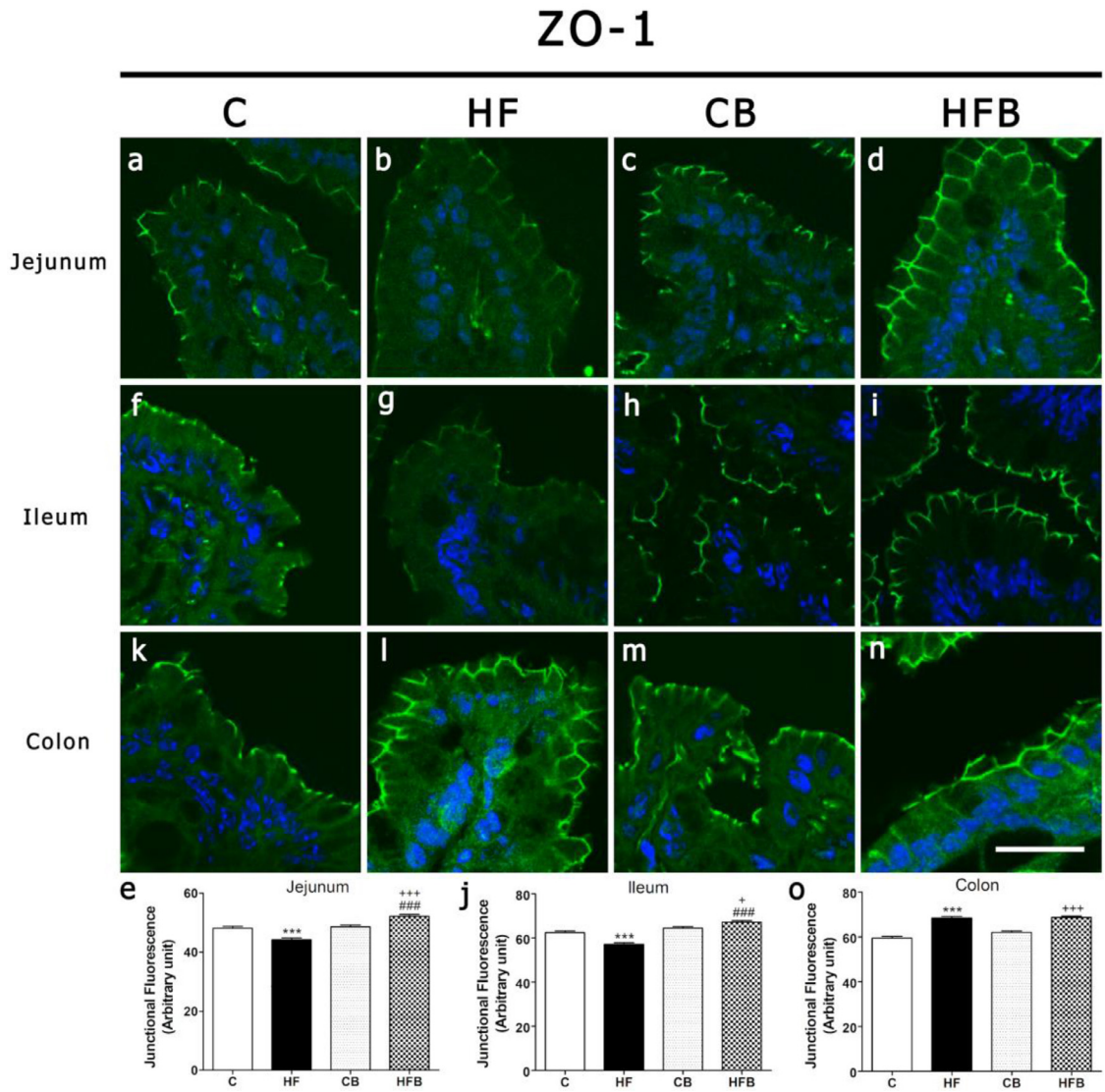


**Fig. 6.** Effect of the dietary supplementation with sodium butyrate on the cellular distribution of ZO-1 in the epithelium of small intestine (jejunum and ileum) and large intestine (colon) of mice fed a standard or high-fat (HF) diet. Images show the immunofluorescence detection of ZO-1 (in green; DAPI/nuclei in blue) in cryosections of intestine segments of mice from the different experimental groups (C/Control, HF/High-fat diet, CB/Control+Butyrate, and HFB/High-fat diet+Butyrate). The analysis of the degree of fluorescence at the cell-cell contact showed that HF diet induced a significant reduction of the ZO-1 content at the intercellular region of the epithelial cells of the jejunum (e) and ileum (j) but led to an increase in the junctional content of this protein in the colon epithelium (o). Butyrate supplementation reversed the effects of the HF diet on the junctional content of this TJ protein in jejunum and ileum (e and j) but not in the colon (o). Compared to the CB group, the HFB group showed a significant increase in ZO-1 in the three studied segments (jejunum-e, ileum-j, colon-o). Bar, 25 $\mu$m. The values of degree of junctional fluorescence represent the means + SEM (5 animals/group, 3 independent experiments).$^{***}P < .0001$ compared to C group, $###P < .0001$ compared to HF group, $+P < .05$ $+++P < .0001$ compared to CB group (one-way ANOVA followed by Bonferroni's post-test).

So, these findings highlight another possible mechanism of butyrate action on the intestinal epithelial barrier during the early stages of T2D, besides its well-known positive effect on gene expression of some TJ proteins through inhibition of the HDAC as described by other *in vitro* and *in vivo* studies [26,33,87–90]. Interestingly, using the Caco-2 cell model of the intestinal epithelium, Peng and colleagues also demonstrated that butyrate incubation did not significantly increase protein expression of claudins, occludin, and ZO-1 but enhanced their location at the cell-cell contact site, facilitating TJ assembly, during a calcium switch assay [91]. This dynamic process involved the activation of the AMP-activated protein kinase (AMPK). Further work is needed to determine the molecular mechanism underlying the effect of butyrate on the TJ barrier in prediabetic mice. Nevertheless, AMPK seems to be a good candidate for a signaling molecule given the fact that it is activated by butyrate in the liver and muscle of diabetic mice [25] and it plays a key structural and regulatory role in cell-cell junctions [92,93].

### *3.3. Exposure to the intestinal luminal content from mice that received butyrate supplementation maintains the TJ structure in Caco-2 cells*

In pioneering work, Oliveira and coworkers (2019) [41] have observed that *in vitro* exposure to the intestinal content, particularly of the small intestine, of mice fed a HF diet induced disruption of the TJ-mediated epithelial barrier in Caco-2 monolayers. This result suggests a possible involvement of a component of the intestinal lumen in the increased intestinal permeability seen *in vivo* after HF-diet intake [59]. Following this idea, we investigated whether

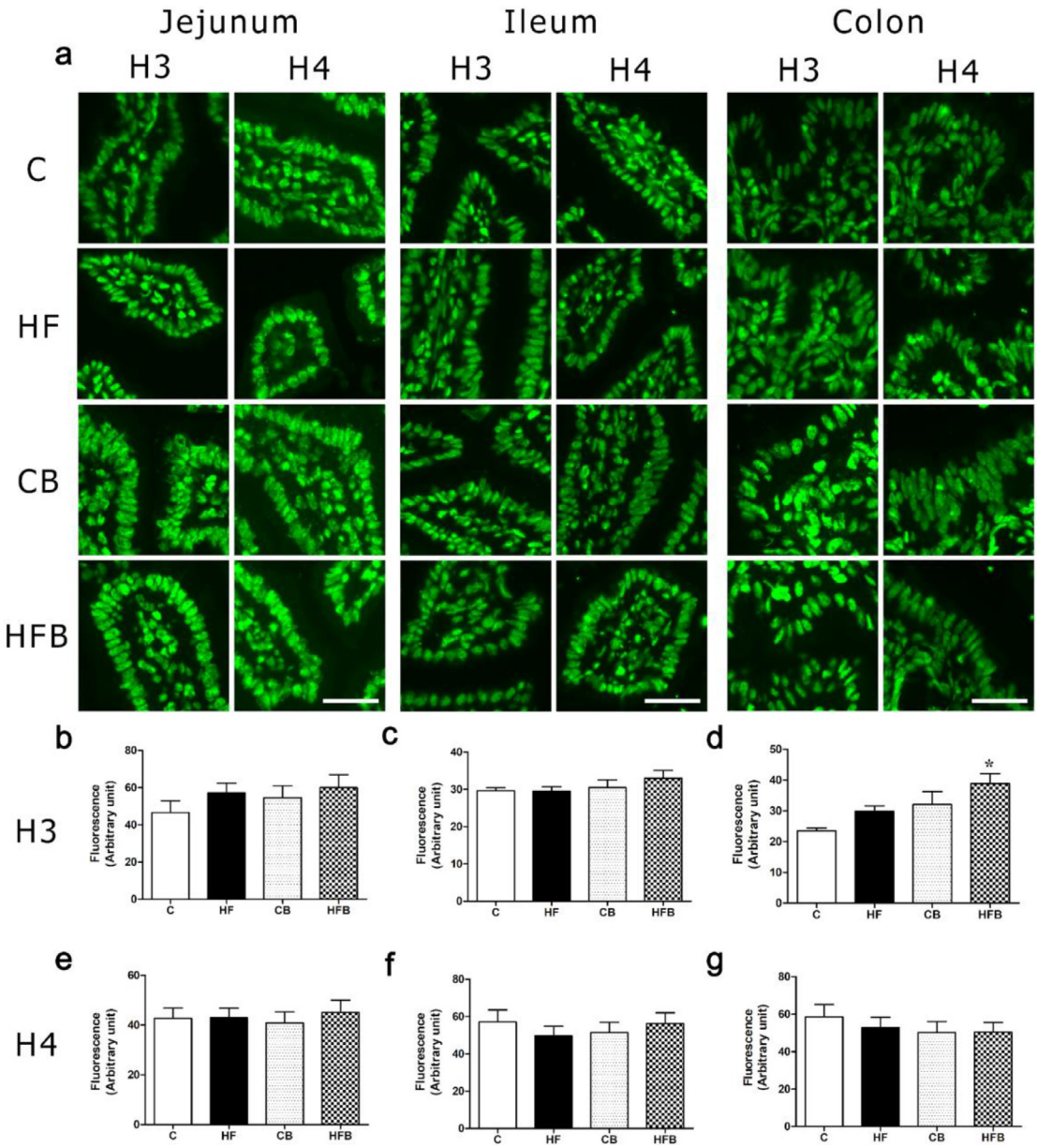


**Fig. 7.** Effect of the dietary supplementation with sodium butyrate in the acetylation level of histones H3 and H4 on the intestine epithelium. The acetylated H3 and H4 were detected by immunofluorescence in cryosections of the epithelium obtained from the small intestine (jejunum and ileum) and large intestine (colon) from all the experimental groups (C/Control, HF/High-fat diet, CB/Control+Butyrate, and HFB/High-fat diet+Butyrate) (a). No significant difference was observed in the degree of acetylation of H3 and H4 among the groups (C, HF, CB, and HFB) (b, c, e, f, g), except in the colon the degree of H3 acetylation in the HFB group was higher compared to C group (d). Bar, 50 $\mu$m. The values of fluorescence degree (expressed as arbitrary units) represent the means + SEM (5 animals/group, 3 independent experiments). $^{*}P < .05$ in relation to the C group (one-way ANOVA followed by Bonferroni's post-test).

the intestinal luminal content from mice fed a diet supplemented with butyrate would also have a protective effect on the epithelial barrier *in vitro*.

As shown in Fig. 9, the exposure of Caco-2 cells to the luminal content of the small intestine from prediabetic mice (HF) did not alter cell viability (Fig. 9a), but resulted in a tendency to decrease the TEER ($P = .06$) (Fig. 9b) associated with a significant increase in paracellular permeability to LY ($P < .05$) (Fig. 9c) when compared to cells exposed to the luminal content from mice that received a standard diet (C) or to Krebs. These changes, indicative of impairment of the paracellular barrier [41,77,94], were accompanied by a significant decrease in the junctional labeling of TJ proteins (claudin-1 and ZO-1) (Fig. 9d), suggesting a disruption of TJ in Caco-2 cells when exposed to the luminal content of small intestine from HF-fed prediabetic mice compared to those exposed to the luminal content from control mice (C). In contrast, cells treated with the intestine luminal content from mice receiving butyrate (either with a high-fat diet (HFB) or a standard diet (CB)) maintained the TEER values close to those of cells exposed to the intestine luminal content of mice that received a standard diet (C), as well as showed the restoration of paracellular permeability at similar levels to those of cells exposed to Krebs (Fig. 9b and c).

Corroborating these functional data, immunofluorescence analyses showed that cells exposed to the intestine luminal content from mice treated with butyrate supplementation reestablished the typical structure of TJ, with immunostaining for Cld-1 and ZO-

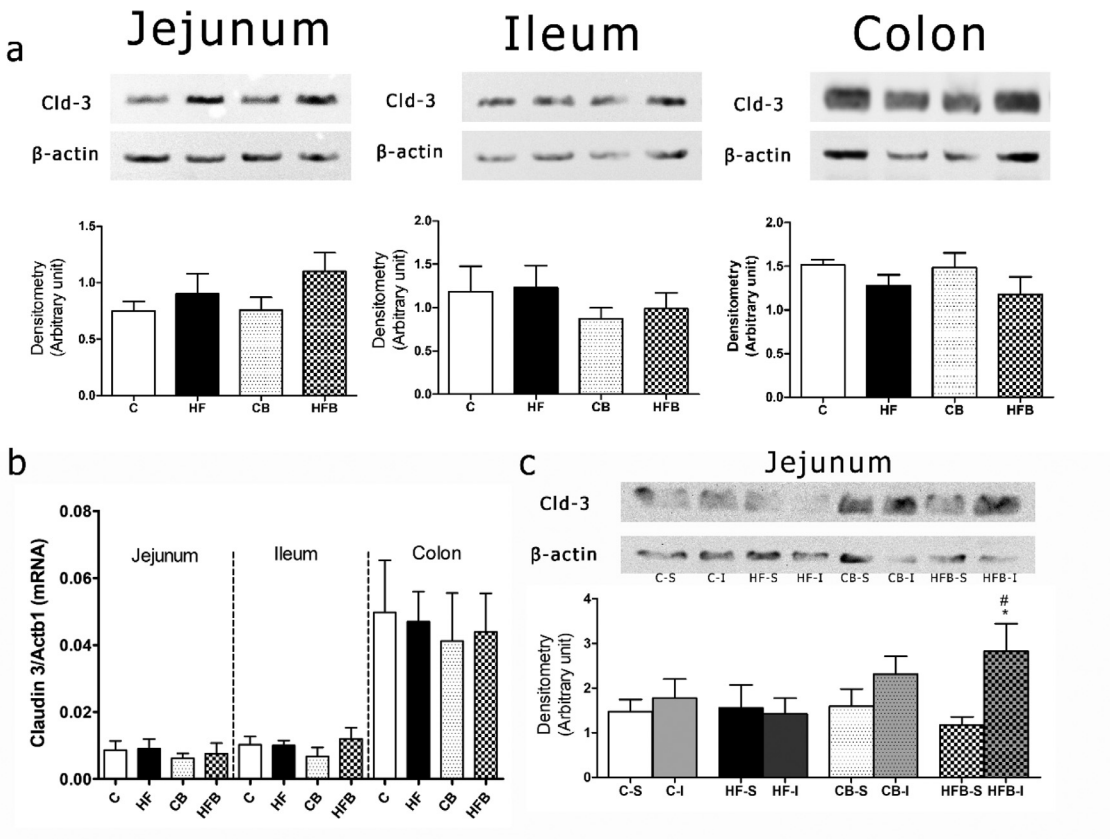


**Fig. 8.** The effect of dietary supplementation with sodium butyrate on Claudin-3 (Cld-3) gene expression, total cell protein content, and junctional/cytoplasm fractions in intestinal epithelium from prediabetic mice. Cld-3 gene expression (b) and cell protein content (a) were assessed by absolute qPCR and immunoblotting, respectively, in epithelium homogenates obtained from the jejunum, ileum, and colon segments of all experimental groups (C/Control, HF/High-fat diet, CB/Control+Butyrate, and HFB/High-fat diet+Butyrate). For junctional/cytoplasm fractions (c), jejunum homogenates were prepared to obtain Triton X-100-soluble (S)(cytoplasmic) and Triton X-100-insoluble (I)(junctional) fractions and then processed for immunoblotting to reveal Cld-3. Graphs a and b show the values of the ratio between TJ protein signal/$\beta$-actin band densitometry or TJ protein/total protein (Ponceau) band densitometry. No significant difference was observed in the protein content (a) and gene expression (b) of Cld-3 among the groups. Nevertheless, we note an increase in the TJ protein content associated with the Triton X-100-insoluble fraction, which represents the protein pool associated with the junctional membrane site, in the HF-fed animals treated with butyrate (HFB) in comparison with those that did not receive this SCFA (HF) (c). This indicates a reinforcement of the intestinal barrier with butyrate particularly in prediabetic mice. The values in a and c represent the means + SEM of the ratio between Cld-3/$\beta$-actin or Cld-3/total protein (Ponceau) band densitometry (4–6 animals/group, 2–3 independent experiments). Values in b represent the means + SEM of the ratio between *Cld-3/Actb1* expression (5–7 animals/group, 2 independent experiments). $^{*}P < .05$ HFB-I fraction in relation to the HFB-S fraction group; $\#P < .05$ HFB-I group in relation to the HF-I group (one-way ANOVA followed by Bonferroni's post-test).

1 like those of cells that were exposed to the luminal content from control mice or Krebs (Fig. 9d). These changes in the junctional distribution of TJ proteins were not accompanied by significant alterations in Cld-1, Occludin, and ZO-1 cell content in Caco-2 cells, as revealed by immunoblotting (Fig. 9e–g). Altogether, these results are in accordance with our previous work [41] and demonstrate that there is a direct association between altered components of the intestinal luminal content and integrity of the intestinal epithelial barrier during type 2 prediabetes in mice, which is reversed with butyrate supplementation. By reproducing the *in vivo* actions of the butyrate on the intestinal epithelial barrier, this *in vitro* Caco-2 model can provide an interesting tool to further investigate the cellular and molecular mechanisms of butyrate on the TJ barrier during type 2 prediabetes.

### *3.4. Sodium butyrate has no further effect on the plasma/serum and intestinal levels of LPS, zonulin, TNF-α, or IL-6 at the prediabetic state*

Based on evidence suggesting an anti-inflammatory effect of butyrate [39,40,89,95], we investigated whether butyrate would have any effect on the systemic/tissue levels of some inflammatory markers (*i.e.*, LPS, zonulin, TNF-$\alpha$, and IL-6) during type 2 prediabetes.

The link between T2D and a systemic low-grade inflammation state is well established [5,45,96]. Studies have shown that diabetic patients and animal models display an increase in the blood level of LPS, zonulin, and proinflammatory cytokines [45,97], although endotoxemia (high systemic level of LPS) and inflammation may not be detected in the prediabetic state [58]. It has been proposed that a dysfunction of the intestinal epithelial barrier would promote the transepithelial passage of LPS resulting in endotoxemia, which contributes to the development of peripheral insulin resistance in T2D [15,19,45]. Zonulin, in turn, an endogenous molecule secreted by several cell types that increases intestinal permeability [44,45,98], would facilitate the transport of luminal antigens, stimulating an immune response and the release of proinflammatory cytokines, such as TNF-$\alpha$, and IL-6, by macrophages and adipocytes [38,99].

In the present study, neither the administration of the HF diet nor the supplementation with butyrate significantly altered the concentration of the pro-inflammatory cytokines TNF-$\alpha$ (Fig. 10a–c) and IL-6 (Fig. 10d–f), or LPS (Fig. 10g–i) and zonulin (Fig. 10j

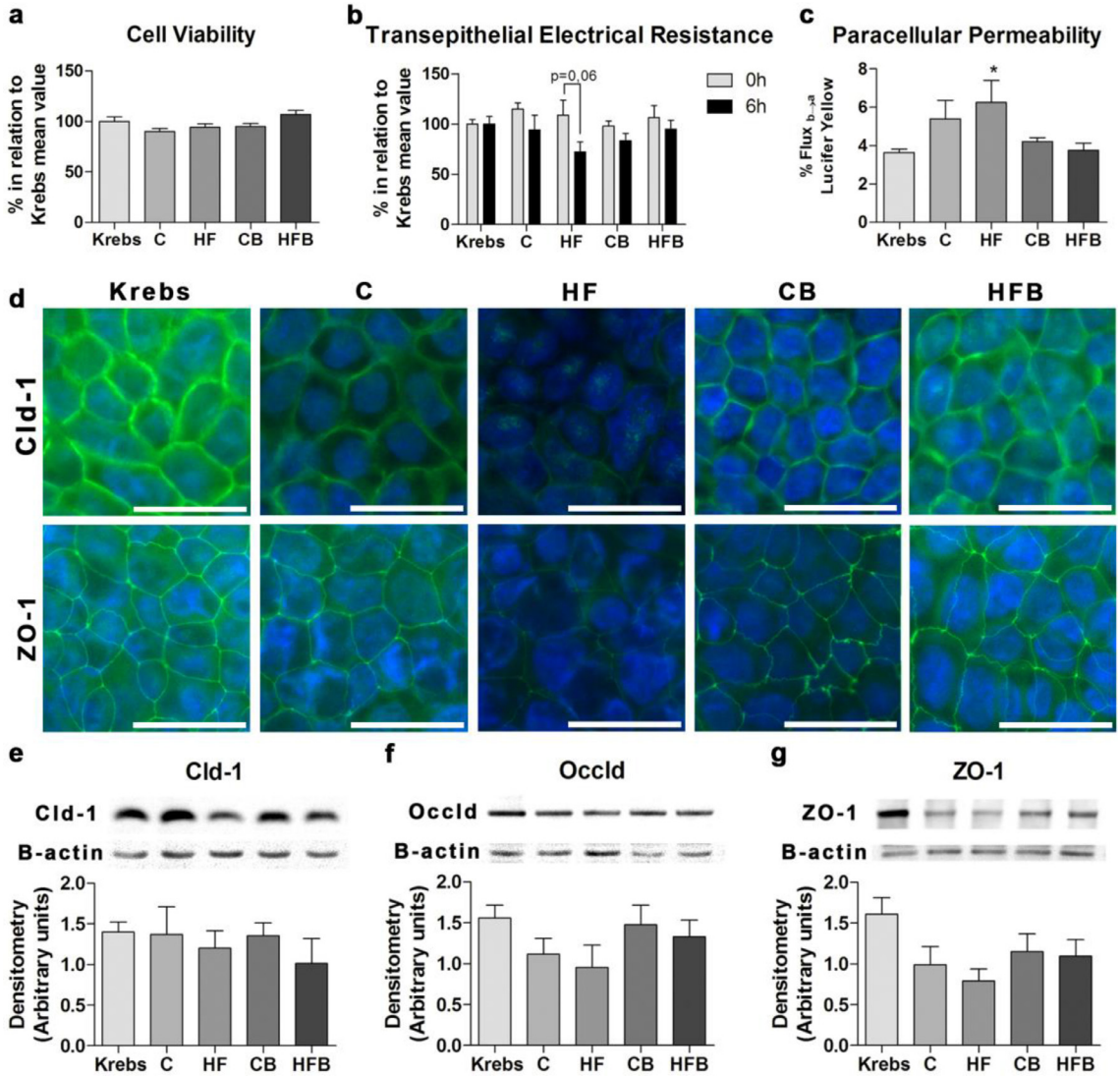


**Fig. 9.** Exposure of Caco-2 monolayers to the luminal content of small intestine isolated from mice from the different experimental groups. (a) Cell viability, (b) transepithelial electrical resistance (TEER), (c) paracellular permeability to Lucifer Yellow (LY), and (d) intercellular distribution of tight junctional proteins (claudin-1 and ZO-1) were evaluated in Caco-2 monolayers after 6 h-exposure to Krebs buffer or to the luminal content of small intestine from mice of different groups (C/Control, HF/High-fat diet, CB/Control+Butyrate, and HFB/High-fat diet+Butyrate). Cell viability was assessed by the Neutral Red assay. The images in (d) are representative of Caco-2 monolayers immunolabeled for claudin-1 and ZO-1 (in green - FITC; DAPI/nuclei in blue) (e, f, g) Immunoblotting for junctional proteins (claudin-1 - Cld-1, occludin - Occld, and ZO-1) in homogenates of Caco-2 monolayers exposed to the luminal intestine contents using the beta-actin as the loading control. Exposure of Caco-2 monolayers to luminal small intestine content of prediabetic mice (HF) induced a significant reduction in TEER (b) as well as an increase in LY paracellular permeability (c) that was associated with a marked decrease in junctional immunodetection of Cld-1 and ZO-1, indicative of disruption of the epithelial paracellular barrier (d). These changes in the structure and function of TJ were not observed when the cells were treated with the luminal intestine content of HF-fed mice receiving butyrate (CB and HFB). Immunoblotting shows no alteration in the total cell content of the TJ proteins studied (e-g). Graphs in e-g display the mean values + SEM (4 membranes/group, two independent experiments) of the optical density analysis of the TJ protein bands. Results in a-c are expressed as means + SEM (in a, 12–21 monolayers/group; in b and c, 6–8 monolayers/group, 2 independent experiments). $^{*}P < .05$ in relation to Krebs (one-way ANOVA followed by Bonferroni's post-test).

and k) in plasma/serum, adipose tissue and/or intestine of mice from the different experimental groups (C, HF, CB, HFB). Normal plasma/intestinal LPS levels observed herein indicate that our type 2 prediabetes mice model did not develop endotoxemia, while normal plasma and adipose/intestinal levels of zonulin and TNF-$\alpha$/IL-6 suggest an absence of marked general systemic and intestinal inflammatory state mediated by these molecules in the animals, which agrees with our previous work [31,58]. Taken altogether, our data show that butyrate treatment has no further effect on the level of these markers in the context of prediabetes.

Therefore, the benefits of diet supplementation with butyrate on insulin resistance, energy metabolism, and intestinal barrier in prediabetic mice, as reported herein and in previous work [31], cannot be explained by its potential anti-inflammatory actions. This is a novel finding since several works have attributed the metabolic improvement of diabetic animals to the reduction of the endotoxemia and low-grade inflammation state seen after butyrate treatment [89,90,95,100–102]. Instead, our results indicate that, at the early stages of T2D, the metabolic effect of butyrate on peripheral tissues (*i.e.*, brown/white adipose tissue, muscle, liver), not on systemic/local inflammation, may play a more important role in its protective actions against obesity and diabetes-related insulin resistance and glucose and lipid metabolism disturbances. These butyrate effects may include increases in the AMPK/PGC-

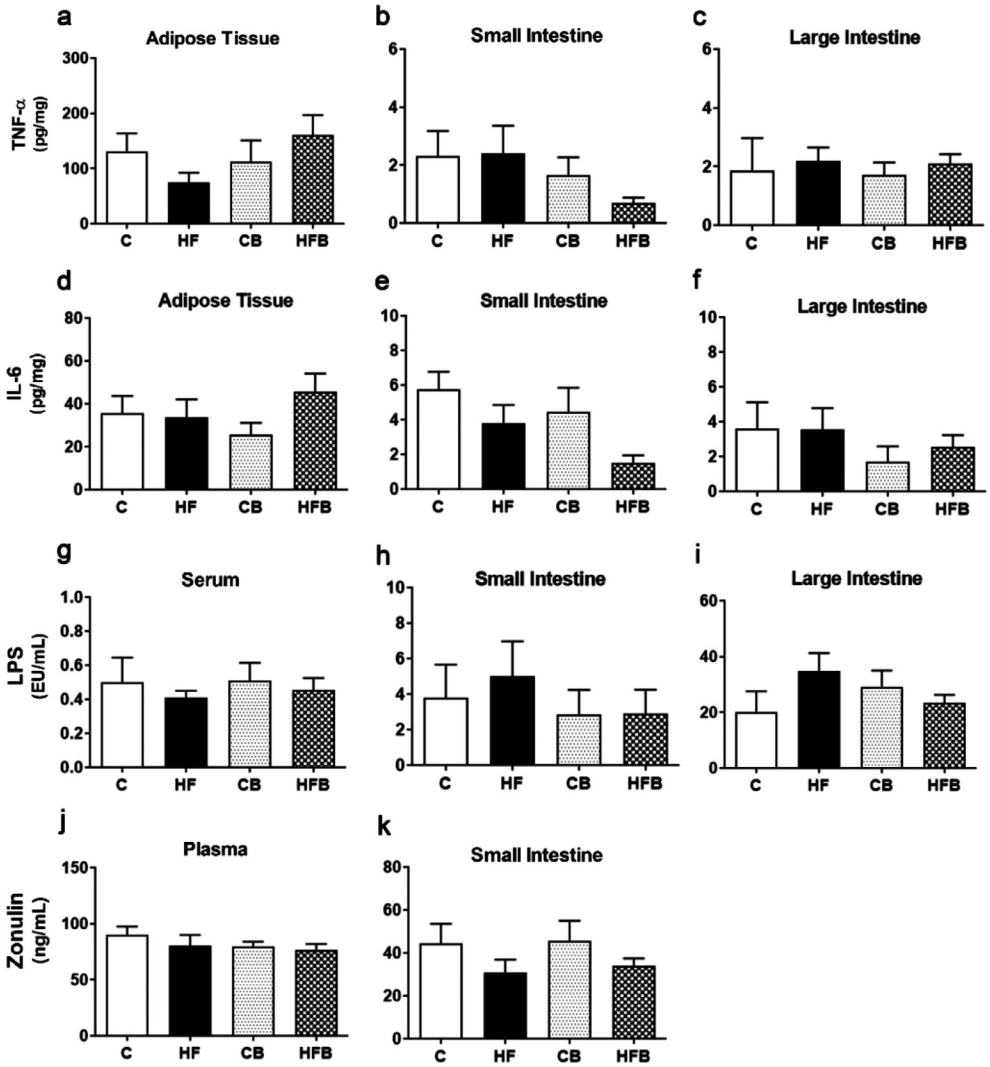


**Fig. 10.** Effect of the dietary supplementation with sodium butyrate on LPS, zonulin, TNF-$\alpha$, and IL-6 quantification in serum/plasma, adipose tissue, and intestine of mice fed a standard or a high-fat diet. No significant difference was observed in the concentration of TNF-$\alpha$ and IL-6 in adipose tissue (a and d) and intestine (b, c, e, f) neither in serum/plasma and intestinal concentrations of LPS (g–i) and zonulin (j and k) among the experimental groups (C/Control, HF/High-fat diet, CB/Control+Butyrate, and HFB/High-fat diet+Butyrate). The values represent the means + SEM ($n$ = 6–9 animals/group, 2 independent experiments).

1$\alpha$-induced $\beta$-oxidation of lipids in WAT and liver [25,67,100,102], the oxidative mitochondrial capacity in muscles [25,67,100,102], the BAT thermogenesis [25,102] (Fig. 2g–i), and the gut secretion of GLP-1 (that increase insulin secretion and sensitivity) [100,102,103], as well as a decrease in ectopic deposition of lipids in the liver, muscle and pancreas (associated with an enhancement of insulin sensitivity) [22,31,100].

### *3.5. Butyrate supplementation does not present systemic toxicity and attenuates liver dysfunction marker and lymphocytosis induced by the high-fat diet*

Given the possible therapeutic use of butyrate as an adjunct in the treatment of metabolic and intestinal diseases, we look at the possible systemic toxicity of sodium butyrate by evaluating the red and white blood cell count and the biochemical profile for markers of liver function (ALT and AST), pancreatic (amylase) and renal (creatinine) in mice from the different groups (C, HF, CB, and HFB) (Table 1). The hematological analysis showed no changes in the hematocrit, red blood cell, and platelet count in mice from the different groups. However, the HF group showed a significant increase ($P < .05$) in hemoglobin levels compared to the C group, with no changes in the other groups (Table 1). There was also a significant increase in the total leukocyte count ($P < .05$) and specifically in the lymphocytes ($P < .05$) in the HF group compared to the C group, with no changes in the other groups (CB and HFB), indicating inhibition of lymphocytosis with treatment by sodium butyrate. In biochemical analyses, a significant increase in the blood level of ALT, a liver function marker, was observed in the HF group compared to the C group, and supplementation with sodium butyrate significantly reduced this change in the HFB group compared to the HF group mice. The latter result corroborates our previous work showing that supplementation with sodium butyrate inhibits the hepatic steatosis developed in HF diet-fed prediabetic mice [31]. Yet, there was no significant alteration in the other investigated biochemical parameters (AST, creatinine, and amylase) among the groups (Table 1). Overall, butyrate seems to display no toxic effect besides ameliorating some blood parameters.

Table 1
Hematology analysis and biochemical parameters

| | Control | High-fat diet | Control+B | High-fat+B |
|---|---|---|---|---|
| *Creatinine (mg/dL)* | 0.37 ± 0.10 | 0.24 ± 0.12 | 0.34 ± 0.08 | 0.39 ± 0.08 |
| *ALT (U/L)* | 37 ± 4.63 | 105 ± 10.48† | 33 ± 3.80 | 46 ± 7.86‡ |
| *AST (U/L)* | 219 ± 39 | 279 ± 43 | 268 ± 46 | 223 ± 46 |
| *Amylase (U/mL)* | 1.00 ± 0.12 | 1.05 ± 0.12 | 0.99 ± 0.15 | 0.95 ± 0.08 |
| *Hematocrit (%)* | 36 ± 0.82 | 38 ± 0.63 | 38 ± 0.90 | 37 ± 0.36 |
| *Hemoglobin (g/dL)* | 11 ± 0.52 | 13 ± 0.24* | 12 ± 0.29 | 12 ± 0.29 |
| *Erythrocytes ($x10^6/\mu L$)* | 8.44 ± 0.40 | 9.02 ± 0.15 | 9.08 ± 0.26 | 8.90 ± 0.19 |
| *Leucocytes (cells/$\mu L$)* | 3713 ± 484 | 6160 ± 446* | 4057 ± 889 | 4860 ± 593 |
| *Neutrophils (cells/$\mu L$)* | 1080 ± 175 | 1417 ± 251 | 1181 ± 311 | 1355 ± ± 261 |
| *Lymphocytes (cells/$\mu L$)* | 2514 ± 340 | 4566 ± 410* | 2771 ± 603 | 3426 ± 409 |
| *Platelets ($x10^6/\mu L$)* | 1.21 ± 0.09 | 1.25 ± 0.07 | 1.31 ± 0.09 | 1.46 ± 0.15 |

Values are expressed as mean ± SEM ($n$ = 5–10 animals/group; 4 independent experiments).
* $P < .05$ in relation to Control.
† $P < .0001$ in relation to Control.
‡ $P < .0001$ in relation to HF.

## 4. Conclusions

The present work demonstrated that butyrate treatment has no effect on lean control mice concerning the parameters analyzed (glycemia, glucose tolerance, lipidemia, fat/lean masses, basal metabolism, WAT and BAT depot, and TJ-mediated intestinal epithelial barrier integrity), which suggests that this SCFA acts mainly when animals are challenged by a HF diet. In the context of prediabetes, sodium butyrate protects against HF diet-induced body weight gain and fat/lean mass ratio imbalance, it restores basal energy expenditure and the integrity of *in vivo* and *in vitro* intestinal epithelial barrier, as well as preserves the morphological and some molecular features of BAT in type 2 prediabetic mice. These positive effects of butyrate occur independently of the recognized anti-inflammatory and/or epigenetic actions of this SCFA, suggesting that the metabolic action of butyrate on peripheral tissues/organs is more important at this stage of T2D. Regarding its action on intestinal TJ, we demonstrated, for the first time, that butyrate induces the trafficking of TJ proteins to the cell-cell contact region of the epithelia, thereby reinforcing barrier function. Therefore, we provide further evidence of the beneficial effect of butyrate administration to prevent the metabolic and intestinal dysfunction associated with type 2 prediabetes.

## Author Statement

The authors declare that the work described has not been published previously (except in the form of an abstract, a published lecture or academic thesis), that it is not under consideration for publication elsewhere, and that its publication is approved by all authors.

## Data availability

Data will be made available on request.

## Declaration of Competing Interest

The authors declare that they have no conflict of interest.

## CRediT authorship contribution statement

**Valquiria A. Matheus:** Conceptualization, Investigation, Formal analysis, Visualization, Data curation, Writing – original draft. **Ricardo B. Oliveira:** Investigation, Formal analysis, Writing – review & editing. **Daniela A. Maschio:** Investigation, Formal analysis, Writing – review & editing. **Susely F.S. Tada:** Investigation, Formal analysis, Writing – review & editing. **Gabriela M. Soares:** Investigation, Formal analysis, Writing – review & editing. **Felippe Mousovich-Neto:** Investigation, Formal analysis, Writing – review & editing. **Raul G. Costa:** Investigation, Formal analysis, Writing – review & editing. **Marcelo A. Mori:** Resources, Writing – review & editing. **Helena C.L. Barbosa:** Conceptualization, Writing – review & editing. **Carla B. Collares-Buzato:** Conceptualization, Formal analysis, Supervision, Funding acquisition, Writing – original draft, Writing – review & editing.

## Acknowledgments

The authors thank Prof. Valéria H. A. C. Quitete, Prof. Elaine Minatel and Prof. Alexandre Leite Rodrigues de Oliveira for allowing access to the laboratory facilities.

## Supplementary materials

Supplementary material associated with this article can be found, in the online version, at doi:10.1016/j.jnutbio.2023.109409.

## References

[1] World Health Organization, "Global report on diabetes," *Isbn 9789241565257*, 978, 88, 2016.
[2] Montanya E. Insulin resistance compensation: not just a matter of $\beta$-cells? Diabetes 2014;63(3):832–4. doi:10.2337/db13-1843.
[3] Collares-Buzato CB. High-fat diets and $\beta$-cell dysfunction: molecular aspects. In: Mauricio D, editor. Molecular Nutrition and Diabetes. Elsevier; 2016. p. 115–30.
[4] Banerjee S, Talukdar I, Banerjee A, Gupta A, Balaji A, Aduri R. Review type II diabetes mellitus and obesity: common links, existing therapeutics and future developments. J Biosci 2019;44(150):1–13. doi:10.1007/s12038-019-9962-7.
[5] Tsalamandris S, Antonopoulos AS, Oikonomou E, Papamikroulis GA, Vogiatzi G, Papaioannou S, et al. The role of inflammation in diabetes: current concepts and future perspectives. Eur Cardiol Rev 2019;14(1):50–9. doi:10.15420/ecr.2018.33.1.
[6] Tangvarasittichai S. Oxidative stress, insulin resistance, dyslipidemia and type 2 diabetes mellitus. World J Diabetes 2015;6(3):456–80. doi:10.4239/wjd.v6.i3.456.
[7] Cypess AM, Kahn CR. Brown fat as a therapy for obesity and diabetes Aaron. Curr Opin Endocrinol Diabetes Obes 2010;17(2):143–9. doi:10.1097/MED.0b013e328337a81f.
[8] Neu J, Reverte CM, Mackey AD, Liboni K, Tuhacek-Tenace LM, Hatch M, et al. Changes in intestinal morphology and permeability in the biobreeding rat before the onset of type 1 diabetes. J Pediatr Gastroenterol Nutr 2005;40:589–95. doi:10.1097/01.mpg.0000159636.19346.c1.

[9] De Kort S, Keszthelyi D, Masclee AAM. Leaky gut and diabetes mellitus: what is the link? Obes Rev 2011;12(6):449–58. doi:10.1111/j.1467-789X.2010.00845.x.
[10] Everard A, Cani P. Diabetes, obesity and gut microbiota. Best Pract Res Clin Gastroenterol 2013;27(1):73–83. doi:10.1016/j.bpg.2013.03.007.
[11] Scheithauer TPM, Dallinga-Thie GM, de Vos WM, Nieuwdorp M, van Raalte DH. Causality of small and large intestinal microbiota in weight regulation and insulin resistance. Mol Metab 2016;5(9):759–70. doi:10.1016/j.molmet.2016.06.002.
[12] Sabatino A, Regolisti G, Karupaiah T, Sahathevan S, Singh BKS, Khor BH, et al. Protein-energy wasting and nutritional supplementation in patients with end-stage renal disease on hemodialysis. Clin Nutr 2017;36(3):663–71. doi:10.1016/j.clnu.2016.06.007.
[13] Spiljar M, Merkler D, Trajkovski M. The immune system bridges the gut microbiota with systemic energy homeostasis: Focus on TLRs, mucosal barrier, and SCFAs. Front Immunol 2017;8:1–10. doi:10.3389/fimmu.2017.01353.
[14] Geurts L, Neyrinck AM, Delzenne NM, Knauf C, Cani PD. Gut microbiota controls adipose tissue expansion, gut barrier and glucose metabolism: Novel insights into molecular targets and interventions using prebiotics. Benef Microbes 2014;5(1):3–17. doi:10.3920/BM2012.0065.
[15] Gomes JMG, de Costa JA, de Alfenas RCG. Metabolic endotoxemia and diabetes mellitus: a systematic review. Metabolism 2017;68:133–44. doi:10.1016/j.metabol.2016.12.009.
[16] Buckley A, Turner JR. Cell biology of tight junction barrier regulation and mucosal disease. Cold Spring Harb Perspect Biol 2018;10(1):a029314. doi:10.1101/cshperspect.a029314.
[17] Gunzel D, Yu ASL. Claudins and the modulation of tight junction permeability. Physiol Rev 2013;93(2):525–69. doi:10.1152/physrev.00019.2012.
[18] Krug SM, Schulzke JD, Fromm M. Tight junction, selective permeability, and related diseases. Semin Cell Dev Biol 2014;36:166–76. doi:10.1016/j.semcdb.2014.09.002.
[19] Odenwald MA, Turner JR. The intestinal epithelial barrier: a therapeutic target? Nat Rev Gastroenterol Hepatol 2016;14(1):9–21. doi:10.1038/nrgastro.2016.169.
[20] Kahn SE, Hull RL, Utzschneider KM. Mechanisms linking obesity to insulin resistance and type 2 diabetes. Nature 2006;444(7121):840–6. doi:10.1038/nature05482.
[21] Shoelson SE, Lee J, Goldfine AB, Shoelson SE, Lee J, Goldfine AB. Inflammation and insulin resistance. J Clin Invest 2006;116(7):1793–801. doi:10.1172/JCI29069.
[22] Khan S, Jena G. Sodium butyrate reduces insulin-resistance, fat accumulation and dyslipidemia in type-2 diabetic rat: a comparative study with metformin. Chem Biol Interact 2016;254:124–34. doi:10.1016/j.cbi.2016.06.007.
[23] Miao W, Wu X, Wang K, Wang W, Wang Y, Li Z, et al. Sodium butyrate promotes reassembly of tight junctions in Caco-2 monolayers involving inhibition of MLCK/MLC2 pathway and phosphorylation of PKC$\beta$2. Int J Mol Sci 2016;17(10):1–12. doi:10.3390/ijms17101696.
[24] Mollica MP, Raso GM, Cavaliere G, Trinchese G, De Filippo C, Aceto S, et al. Butyrate regulates liver mitochondrial function, efficiency, and dynamics in insulin-resistant obese mice. Diabetes 2017;66(5):1405–18. doi:10.2337/db16-0924.
[25] Gao Z, Yin J, Zhang J, Ward RE, Martin RJ, Lefevre M, et al. Butyrate improves insulin sensitivity and increases energy expenditure in mice. Diabetes 2009;58(7):1509–17. doi:10.2337/db08-1637.
[26] Canani RB, Di Costanzo M, Leone L, Pedata M, Meli R, Calignano A. Potential beneficial effects of butyrate in intestinal and extraintestinal diseases. World J Gastroenterol 2011;17(12):1519–28. doi:10.3748/wjg.v17.i12.1519.
[27] Canfora EE, Jocken JW, Blaak EE. Short-chain fatty acids in control of body weight and insulin sensitivity. Nat Rev Endocrinol 2015;11(10):577–91. doi:10.1038/nrendo.2015.128.
[28] Den Besten G, Bleeker A, Gerding A, Van Eunen K, Havinga R, Van Dijk T, et al. Short-chain fatty acids protect against high-fat diet-induced obesity via a PPARG-dependent switch from lipogenesis to fat oxidation. Diabetes 2015;64(7):2398–408. doi:10.2337/db14-1213.
[29] Pelgrim CE, Franx BAA, Snabel J, Kleemann R, Arnoldussen IAC, Kiliaan AJ. Butyrate reduces HFD-induced adipocyte hypertrophy and metabolic risk factors in Obese LDLr-/-.Leiden mice. Nutrients 2017;9(7):1–15. doi:10.3390/nu9070714.
[30] Li Z, Yi C-X, Katiraei S, Kooijman S, Zhou E, Chung C-K, et al. Butyrate reduces appetite and activates brown adipose tissue via the gut-brain neural circuit. Gut 2018;67(7):1269–79. doi:10.1136/gutjnl-2017-314050.
[31] Matheus VA, Monteiro LCS, Oliveira RB, Maschio DA, Collares-Buzato CB. Butyrate reduces high-fat diet-induced metabolic alterations, hepatic steatosis and pancreatic beta cell and intestinal barrier dysfunctions in prediabetic mice. Exp Biol Med 2017;242(12):1214–26. doi:10.1177/1535370217708188.
[32] Rabbani GH, Teka T, Zaman B, Majid N, Khatun M, Fuchs GJ. Clinical studies in persistent diarrhea: dietary management with green banana or pectin in Bangladeshi children. Gastroenterology 2001;121:554–60. doi:10.1053/gast.2001.27178.
[33] Wang HB, Wang PY, Wang X, Wan YL, Liu YC. Butyrate enhances intestinal epithelial barrier function via up-regulation of tight junction protein claudin-1 transcription. Dig Dis Sci 2012;57(12):3126–35. doi:10.1007/s10620-012-2259-4.
[34] Kruh J. Effects of sodium butyrate, a new pharmacological agent, on cells in culture. Mol Cell Biochem 1982;42:65–82. doi:10.1007/BF02796360.
[35] Khan S, Jena GB. Protective role of sodium butyrate, a HDAC inhibitor on beta-cell proliferation, function and glucose homeostasis through modulation of p38/ERK MAPK and apoptotic pathways: study in juvenile diabetic rat. Chem Biol Interact 2014;213(1):1–12. doi:10.1016/j.cbi.2014.02.001.
[36] Patnala R, Arumugam TV, Gupta N, Dheen ST. HDAC inhibitor sodium butyrate-mediated epigenetic regulation enhances neuroprotective function of microglia during ischemic stroke. Mol Neurobiol 2017;54(8):6391–411. doi:10.1007/s12035-016-0149-z.
[37] Kumar M, Song H-J, Cho S-K, Balasubramanian S, Choe S-Y, Rho G-J. Effect of histone acetylation modification with sodium butyrate, a histone deacetylase inhibitor, on cell cycle, apoptosis, ploidy and gene expression in porcine fetal fibroblasts. J Reprod Dev 2007;53(4):903–13. doi:10.1262/jrd.18180.
[38] Ammon HPT. Boswellic extracts and 11-keto-ß-boswellic acids prevent type 1 and type 2 diabetes mellitus by suppressing the expression of proinflammatory cytokines. Phytomedicine 2019;63:1–7. doi:10.1016/j.phymed.2019.153002.
[39] Ohira H, Fujioka Y, Katagiri C, Mamoto R, Aoyama-Ishikawa M, Amako K, et al. Butyrate attenuates inflammation and lipolysis generated by the interaction of adipocytes and macrophages. J Atheroscler Thromb 2013;20(5):425–42. doi:10.5551/jat.15065.
[40] Säemann MD, Böhmig GA, Österreicher CH, Burtscher H, Parolini O, Diakos C, et al. Anti-inflammatory effects of sodium butyrate on human monocytes: potent inhibition of IL-12 and up-regulation of IL-10 production. FASEB J 2000;14(15):2380–2. doi:10.1096/fj.00-0359fje.
[41] Oliveira RB, Canuto LP, Collares-Buzato CB. Intestinal luminal content from high-fat-fed prediabetic mice changes epithelial barrier function in vitro. Life Sci 2019;216:10–21. doi:10.1016/j.lfs.2018.11.012.
[42] Sambuy Y, De Angelis I, Ranaldi G, Scarino ML, Stammati A, Zucco F. The Caco-2 cell line as a model of the intestinal barrier: influence of cell and culture-related factors on Caco-2 cell functional characteristics. Cell Biol Toxicol 2005;21(1):1–26. doi:10.1007/s10565-005-0085-6.
[43] Cani PD, Bibiloni R, Knauf C, Neyrinck AM, Delzenne NM. Changes in gut microbiota control metabolic diet–induced obesity and diabetes in mice. Diabetes 2008;57(6):1470–81. doi:10.2337/db07-1403.
[44] Fasano A. Zonulin, regulation of tight junctions, and autoimmune diseases. Ann N Y Acad Sci 2012;1258(1):25–33. doi:10.1111/j.1749-6632.2012.06538.x.
[45] Jayashree B, Bibin YS, Prabhu D, Shanthirani CS, Gokulakrishnan K, Lakshmi BS, et al. Increased circulatory levels of lipopolysaccharide (LPS) and zonulin signify novel biomarkers of proinflammation in patients with type 2 diabetes. Mol Cell Biochem 2014;388:203–10. doi:10.1007/s11010-013-1911-4.
[46] Falcão VTFL, Maschio DA, Fontes CC, Oliveira RB, Santos–Silva JC, Almeida ACS, et al. Reduced insulin secretion function is associated with pancreatic islet redistribution of cell adhesion molecules (CAMs) in diabetic mice after prolonged high-fat diet. Histochem Cell Biol 2016;146(1):13–31. doi:10.1007/s00418-016-1428-5.
[47] Oliveira RB, Maschio DA, Carvalho CPF, Collares-Buzato CB. Influence of gender and time diet exposure on endocrine pancreas remodeling in response to high fat diet-induced metabolic disturbances in mice. Ann Anat 2015;200:88–97. doi:10.1016/j.aanat.2015.01.007.
[48] Carvalho CPF, Oliveira RB, Britan A, Santos-Silva JC, Boschero AC, Meda P, et al. Impaired $\beta$-cell-$\beta$-cell coupling mediated by Cx36 gap junctions in prediabetic mice. Am J Physiol Endocrinol Metab 2012;303(1):E144–51. doi:10.1152/ajpendo.00489.2011.
[49] Branco RCS, Camargo RL, Batista TM, Vettorazzi JF, Lubaczeuski C, Bomfim LHM, et al. Protein malnutrition mitigates the effects of a high-fat diet on glucose homeostasis in mice. J Cell Physiol 2019;234(5):6313–23. doi:10.1002/jcp.27361.
[50] Raposo HF, Paiva AA, Kato LS, De Oliveira HCF. Apolipoprotein CIII overexpression exacerbates diet-induced obesity due to adipose tissue higher exogenous lipid uptake and retention and lower lipolysis rates. Nutr Metab (Lond) 2015;12(61):1–10. doi:10.1186/s12986-015-0058-6.
[51] Santos RDS, Camargo RL, Vanzela EC, Batista TM, Morato PN. Diet–induced glucose homeostasis dysregulation is enhanced by taurine supplementation in ovariectomized mice. Amino Acids 2018;50(3):469–77. doi:10.1007/s00726-017-2533-z.
[52] Soares GM, Zangerolamo L, Costa-Júnior JM, Vettorazzi JF, Carneiro EM, Saad ST, et al. Whole-body ArhGAP21-deficiency improves energetic homeostasis in lean and obese mice. Front Endocrinol (Lausanne) 2019;10(5):1–9. doi:10.3389/fendo.2019.00338.
[53] Rocha AL, de Lima TI, de Souza GP, Corrêa RO, Ferrucci DL, Rodrigues B, et al. Enoxacin induces oxidative metabolism and mitigates obesity by regulating adipose tissue miRNA expression. Sci Adv 2020;6(49):1–15. doi:10.1126/sciadv.abc6250.
[54] Caminhotto RO, Andreotti S, Komino ACM, Silva FF, Sertié RAL, Christoffolete AM, et al. Physiological concentrations of $\beta$-hydroxybutyrate do not promote adipocyte browning. Life Sci 2019;232:116683. doi:10.1016/j.lfs.2019.116683.
[55] Liu J, Zhu H, Li B, Lee C, Alganabi M, Zheng S, et al. Beneficial effects of butyrate in intestinal injury. J Pediatr Surg 2020;55(6):1088–93. doi:10.1016/j.jpedsurg.2020.02.036.
[56] Kespohl M, Vachharajani N, Luu M, Harb H, Pautz S, Wolff S, et al. The microbial metabolite butyrate induces expression of Th1- associated factors in CD4+ T cells. Front Immunol 2017;8:1–12. doi:10.3389/fimmu.2017.01036.

[57] . In: Doerrier C, Garcia-Souza LF, Krumschnabel G, Wohlfarter Y, Mészáros AT, Gnaiger E, Palmeira C, Moreno A, editors. Mitochondrial Bioenergetics: Methods and Protocols, Methods in Molecular Biology, 1782. New York, NY: Springer Protocols; 2018. p. 31–70. doi:10.1007/978-1-4939-7831-1_3.
[58] Nascimento JC, Matheus VA, Oliveira RB, Tada SFS, Collares-Buzato CB. High-fat diet induces disruption of the tight junction-mediated paracellular barrier in the proximal small intestine before the onset of type 2 diabetes and endotoxemia. Dig Dis Sci 2020;66:3359–74. doi:10.1007/s10620-020-06664-x.
[59] Oliveira RB, Matheus VA, Canuto LP, De Sant'ana A, Collares-Buzato CB. Time-dependent alteration to the tight junction structure of distal intestinal epithelia in type 2 prediabetic mice. Life Sci 2019;238:1–14. doi:10.1016/j.lfs.2019.116971.
[60] Singh AB, Harris RC. Epidermal growth factor receptor activation differentially regulates claudin expression and enhances transepithelial resistance in Madin-Darby canine kidney cells. J Biol Chem 2004;279(5):3543–52. doi:10.1074/jbc.M308682200.
[61] Maschio DA, Matheus VA. Collares-Buzato CB Islet cells are the source of Wnts that can induce beta-cell proliferation in vitro. J Cell Physiol 2019;234(11):19852–65. doi:10.1002/jcp.28584.
[62] Hauschka SD, Konigsberg IR. The influence of collagen on the development of muscle clones. Proc Natl Acad Sci U S A 1966;55(1):119–26. doi:10.1073/pnas.55.1.119.
[63] Zhang W-Q, Zhao T-T, Gui D-K, Gao C-L, Gu J-L, Gan W-J, et al. Sodium butyrate improves liver glycogen metabolism in type 2 diabetes mellitus. J Agric Food Chem 2019;67:7694–705. doi:10.1021/acs.jafc.9b02083.
[64] Jkobsdottira G, Xu J, Molin G, Ahrné S, Nyman M. High-fat diet reduces the formation of butyrate, but increases succinate, inflammation, liver fat and cholesterol in rats, while dietary fibre counteracts these effects. PLoS One 2013;8(11):1–15. doi:10.1371/journal.pone.0080476.
[65] Maschio DA, Oliveira RB, Santos MR, Carvalho CPF, Barbosa-Sampaio HCL, Collares-Buzato CB. Activation of the Wnt/$\beta$-catenin pathway in pancreatic beta cells during the compensatory islet hyperplasia in prediabetic mice. Biochem Biophys Res Commun 2016;478(4):1534–40. doi:10.1016/j.bbrc.2016.08.146.
[66] Rojczyk E, Pałasz A, Wiaderkiewicz R. Effect of short and long-term treatment with antipsychotics on orexigenic/anorexigenic neuropeptides expression in the rat hypothalamus. Neuropeptides 2015;51:31–42. doi:10.1016/j.npep.2015.04.001.
[67] Henagan TM, Stefanska B, Fang Z, Navard AM, Ye J, Lenard NR, Devarshi PP. Sodium butyrate epigenetically modulates high-fat diet-induced skeletal muscle mitochondrial adaptation, obesity and insulin resistance through nucleosome positioning. Br J Pharmacol 2015;172:2782–98. doi:10.1111/bph.13058.
[68] Issekutz B, Birkhead NC, Rodahl K. Use of respiratory quotients in assessment of aerobic work capacity. J Appl Physiol 1962;17(1):47–50. doi:10.1152/jappl.1962.17.1.47.
[69] Kim TN, Park MS, Lim KI, Yang SJ, Yoo HJ, Kang HJ, et al. Skeletal muscle mass to visceral fat area ratio is associated with metabolic syndrome and arterial stiffness: the Korean Sarcopenic Obesity Study (KSOS). Diabetes Res Clin Pract 2011;93(2):285–91. doi:10.1016/j.diabres.2011.06.013.
[70] Srikanthan P, Karlamangla AS. Relative muscle mass is inversely associated with insulin resistance and prediabetes. Findings from the Third National Health and Nutrition Examination Survey. J Clin Endocrinol Metab 2011;96(9):2898–903. doi:10.1210/jc.2011-0435.
[71] Kurinami N, Sugiyama S, Yoshida A, Hieshima K, Miyamoto F, Kajiwara K, et al. Correlation of body muscle/fat ratio with insulin sensitivity using hyperinsulinemic-euglycemic clamp in treatment-naïve type 2 diabetes mellitus. Diabetes Res Clin Pract 2016;120:65–72. doi:10.1016/j.diabres.2016.07.018.
[72] Narita T, Kobayashi M, Itakura K, Itagawa R, Kabaya R, Sudo Y, et al. Differential response to caloric restriction of retroperitoneal, epididymal, and subcutaneous adipose tissue depots in rats. Exp Gerontol 2018;104:127–37. doi:10.1016/j.exger.2018.01.016.
[73] Ricquier D. UCP1, the mitochondrial uncoupling protein of brown adipocyte: a personal contribution and a historical perspective. Biochimie 2017;134:3–8. doi:10.1016/j.biochi.2016.10.018.
[74] Lapa C, Arias-Loza P, Hayakawa N, Wakabayashi H, Werner RA, Chen X, et al. Whitening and impaired glucose utilization of brown adipose tissue in a rat model of type 2 diabetes mellitus. Sci Rep 2017;7(1):5–10. doi:10.1038/s41598-017-17148-w.
[75] Wolever TMS, Chiasson JL. Acarbose raises serum butyrate in human subjects with impaired glucose tolerance. Br J Nutr 2000;84(1):57–61. doi:10.1017/S0007114500001239.
[76] De Vadder F, Kovatcheva-Datchary P, Gonçalves D, Vinera J, Zitoun C, Duchampt A, et al. Microbiota-generated metabolites promote metabolic benefits via gut-brain neural circuits. Cell 2014;156(1–2):84–96. doi:10.1016/j.cell.2013.12.016.
[77] Mongelli-Sabino BM, Canuto LP, Collares-Buzato CB. Acute and chronic exposure to high levels of glucose modulates tight junction-associated epithelial barrier function in a renal tubular cell line. Life Sci 2017;188:149–57. doi:10.1016/j.lfs.2017.09.004.
[78] Volynets V, Reichold A, Bárdos G, Rings A, Bleich A, Bischoff SC. Assessment of the intestinal barrier with five different permeability tests in healthy C57BL/6J and BALB/cJ mice. Dig Dis Sci 2016;61:737–74. doi:10.1007/s10620-015-3935-y.
[79] Garcia-Hernandez V, Quiros M, Nusrat A. Intestinal epithelial claudins: expression and regulation in homeostasis and inflammation. Ann N Y Acad Sci 2017;1397(1):66–79. doi:10.1111/nyas.13360.
[80] Utech M, Mennigen R, Bruewer M. Endocytosis and recycling of tight junction proteins in inflammation. J Biomed Biotechnol 2010;2010:1–6. doi:10.1155/2010/484987.
[81] Butt AM, Khan IB, Hussain M, Idress M, Lu J, Tong Y. Role of post translational modifications and novel crosstalk between phosphorylation and O-beta-GlcNAc modifications in human claudin-1, -3 and -4. Mol Biol Rep 2012;39(2):1359–69. doi:10.1007/s11033-011-0870-7.
[82] Khan N, Asif AR. Transcriptional regulators of claudins in epithelial tight junctions. Hindawi Publ Corp 2015;2015(1):1–6. doi:10.1155/2015/219843.
[83] Hichino A, Okamoto M, Taga S, Akizuki R, Endo S, Matsunaga T, et al. Down-regulation of claudin-2 expression and proliferation by epigenetic inhibitors in human lung adenocarcinoma A549 cells. J Biol Chem 2017;292(6):2411–21. doi:10.1074/jbc.M116.762807.
[84] Stamatovic SM, Johnson AM, Sladojevic N, Keep RF, Andjelkovic AV. Endocytosis of tight junction proteins and the regulation of degradation and recycling. Ann N Y Acad Sci 2017;1397(1):54–65. doi:10.1111/nyas.13346.
[85] Markov AG, Veshnyakova A, Fromm M, Amasheh M, Amasheh S. Segmental expression of claudin proteins correlates with tight junction barrier properties in rat intestine. J Comp Physiol B Biochem Syst Environ Physiol 2010;180(4):591–8. doi:10.1007/s00360-009-0440-7.
[86] Della Ragione F, Criniti V, Pietra V Della, Borriello A, Oliva A, Indaco S, et al. Genes modulated by histone acetylation as new effectors of butyrate activity. FEBS Lett 2001;499(3):199–204. doi:10.1016/s0014-5793(01)02539-x.
[87] Plöger S, Stumpff F, Penner GB, Schulzke JD, Gäbel G, Martens H, et al. Microbial butyrate and its role for barrier function in the gastrointestinal tract. Ann N Y Acad Sci 2012;1258(1):52–9. doi:10.1111/j.1749-6632.2012.06553.x.
[88] Huang C, Song P, Fan P, Hou C, Thacker P, Ma X. Dietary sodium butyrate decreases postweaning diarrhea by modulating intestinal permeability and changing the bacterial communities in weaned piglets. J Nutr 2015;145:2774–80. doi:10.3945/jn.115.217406.
[89] Xu YH, Gao CL, Guo HL, Zhang WQ, Huang W, Tang SS, et al. Sodium butyrate supplementation ameliorates diabetic inflammation in db/db mice. J Endocrinol 2018;238(3):231–44. doi:10.1530/JOE-18-0137.
[90] Yang T, Yang H, Heng C, Wang H, Chen S, Hu Y, et al. Amelioration of non-alcoholic fatty liver disease by sodium butyrate is linked to the modulation of intestinal tight junctions in db/db mice. Food Funct 2020;11(12):10675–89. doi:10.1039/d0fo01954b.
[91] Peng L, Li ZR, Green RS, Holzman IR, Lin J. Butyrate enhances the intestinal barrier by facilitating tight junction assembly via activation of AMP-activated protein kinase in Caco-2 cell monolayers. J Nutr 2009;139(9):1619–25. doi:10.3945/jn.109.104638.
[92] Tsukita K, Yano T, Tamura A, Tsukita S. Reciprocal association between the apical junctional complex and AMPK: a promising therapeutic target for epithelial/endothelial barrier function? Int J Mol Sci 2019;20(23):15–17. doi:10.3390/ijms20236012.
[93] Olivier S, Leclerc J, Grenier A, Tamburini J. Viollet MFB AMPK activation promotes tight junction assembly in intestinal epithelial Caco-2 cells. Int J Mol Sci 2019;20(20):5171. doi:10.3390/ijms20205171.
[94] Canuto LP, Collares-Buzato CB. Increased osmolality enhances the tight junction-mediated barrier function in a cultured renal epithelial cell line. Cell Biol Int 2019;43(1):73–82. doi:10.1002/cbin.11074.
[95] Knudsen KEB, Lærke HN, Hedemann MS, Nielsen TS, Ingerslev AK, Nielsen DSG, et al. Impact of diet-modulated butyrate production on intestinal barrier function and inflammation. Nutrients 2018;10(10). doi:10.3390/nu10101499.
[96] Cani PD, Osto M, Geurts L, Everard A. Involvement of gut microbiota in the development of low-grade inflammation and type 2 diabetes associated with obesity. Gut Microbes 2012;3(4):279–88. doi:10.4161/gmic.19625.
[97] Cani PD, Amar J, Alglesias M, Poggi M, Knauf C, Bastelica D, et al. Metabolic endotoxemia initiates obesity and insulin resistance. Diabetes 2007;56:1761–72. doi:10.2337/db06-1491.
[98] Sturgeon C, Fasano A. Zonulin, a regulator of epithelial and endothelial barrier functions, and its involvement in chronic inflammatory diseases. Tissue Barriers 2016;4(4):1–19. doi:10.1080/21688370.2016.1251384.
[99] Tang Y, Clayburgh DR, Mittal N, Goretsky T, Dirisina R, Zhang Z, et al. Epithelial NF-$\kappa$B enhances transmucosal fluid movement by altering tight junction protein composition after T cell activation. Am J Pathol 2010;176(1):158–67. doi:10.2353/ajpath.2010.090548.
[100] McNabney SM, Henagan TM. Short chain fatty acids in the colon and peripheral tissues: a focus on butyrate, colon cancer, obesity and insulin resistance. Nutrients 2017;9(12):1–28. doi:10.3390/nu9121348.
[101] Baumann A, Jin CJ, Brandt A, Sellmann C, Nier A, Burkard M, et al. Oral supplementation of sodium butyrate attenuates the progression of non-alcoholic steatohepatitis. Nutrients 2020;12(4):1–19. doi:10.3390/nu12040951.
[102] Coppola S, Avagliano C, Calignano A, Canani R Berni. The protective role of butyrate against obesity and obesity-related diseases. Molecules 2021;26(3). doi:10.3390/molecules26030682.
[103] Zhou D, Chen Y-W, Zhao Z-H, Yang R-X, Xin F-Z, Liu X-L, et al. Sodium butyrate reduces high-fat diet-induced non-alcoholic steatohepatitis through upregulation of hepatic GLP-1R expression. Exp Mol Med 2018;50(12):1–12. doi:10.1038/s12276-018-0183-1.